UCRL-17352

University of California

Ernest O. Lawrence Radiation Laboratory

THE INELASTIC SCATTERING OF 17.8-MeV PROTONS FROM ^{58}Ni, ^{60}Ni, AND ^{120}Sn AND THE DETERMINATION OF SPIN AND PARITY ASSIGNMENTS FOR ^{58}Ni FROM α-PARTICLE SCATTERING

Berkeley, California

DISCLAIMER

Submitted to Nucl. Phys.

UCRL-17352
Preprint

UNIVERSITY OF CALIFORNIA

Lawrence Radiation Laboratory
Berkeley, California

AEC Contract No. W-7405-eng-48

THE INELASTIC SCATTERING OF 17.8-MeV PROTONS FROM ^{58}Ni, ^{60}Ni, AND ^{120}Sn AND THE DETERMINATION OF SPIN AND PARITY ASSIGNMENTS FOR ^{58}Ni FROM α-PARTICLE SCATTERING

O. N. Jarvis, B. G. Harvey, D. L. Hendrie, and Jeannette Mahoney

January 1967

UCRL-17352

THE INELASTIC SCATTERING OF 17.8-MeV PROTONS FROM ^{58}Ni, ^{60}Ni, AND ^{120}Sn AND THE DETERMINATION OF SPIN AND PARITY ASSIGNMENTS FOR ^{58}Ni FROM α-PARTICLE SCATTERING

O. N. Jarvis, B. G. Harvey, D. L. Hendrie, and Jeannette Mahoney

Lawrence Radiation Laboratory
University of California
Berkeley, California

January 1967

NUCLEAR REACTIONS ^{58}Ni, ^{60}Ni, ^{120}Sn (p,p'), E = 17.8 MeV; measured $\sigma(E_{p'},\theta)$. Deduced optical model and deformation parameters. ^{58}Ni(α,α'), E = 50.2 MeV; measured $\sigma(E_{\alpha'},\theta)$. Deduced Jπ, deformation parameters. Enriched targets.

UCRL-17352

THE INELASTIC SCATTERING OF 17.8-MeV PROTONS FROM ^{58}Ni, ^{60}Ni, AND ^{120}Sn AND THE DETERMINATION OF SPIN AND PARITY ASSIGNMENTS FOR ^{58}Ni FROM α-PARTICLE SCATTERING*

O. N. Jarvis,** B. G. Harvey, D. L. Hendrie, and Jeannette Mahoney

Lawrence Radiation Laboratory
University of California
Berkeley, California

January 1967

Abstract

Protons of energy about 17.8 MeV were scattered from targets of ^{58}Ni, ^{60}Ni, and ^{120}Sn. Precise angular distributions were obtained over the angular range 20°-170° for most of the low-lying excited states in each nucleus. Also, 50-MeV α particles were scattered from ^{58}Ni to determine the spin-parity assignments for a number of levels. Using these assignments, it was found that the ^{58}Ni proton scattering angular distributions for levels with the same spin and parity demonstrated definite similarities. Optical model studies were made for the proton elastic scattering data and the resulting potentials were used to obtain satisfactory DWBA predictions for the collective 2+ and 3- levels. The proton scattering angular distributions for many of the weaker levels were also found to resemble strongly the collective model DWBA predictions.

---

*This work was performed under the auspices of the U. S. Atomic Energy Commission.

**Permanent address: Atomic Energy Research Establishment, Harwell, Berkshire, England.

1. Introduction

The purpose of the present work was to provide data suitable for detailed comparison with theory, such as the microscopic description of inelastic scattering as developed, for example, by Glendenning and Veneroni[1]). Inelastic scattering of 17.8-MeV protons from the low-lying levels in the nuclei ^{58}Ni, ^{60}Ni, and ^{120}Sn is suitable for this purpose because nuclear wave function calculations have been made[2]), based on the two quasiparticle description of the excited states and with the closed shells regarded as inert. Glendenning and Veneroni have demonstrated that these calculations produce the desired enhancement for the collective 2^+ (single-phonon) levels.

The present choice of proton bombarding energy was such that compound nucleus effects were expected to be small, yet the energy resolution sufficiently good that the scattering from the majority of levels could be clearly resolved. The precise energy was dictated by the fact that elastic scattering polarization data (but no cross-section data) were available[3]) for the nickel isotopes at 17.8 MeV.

Although the locations of the low-lying levels in the nickel and tin isotopes are well-known, information regarding the spins and parities of these levels is far from complete. It is, of course, essential that such information be available before comparison between theory and experiment can be made. For this reason the scattering of 50-MeV α particles from ^{58}Ni was studied, resulting in new assignments for many levels. Unfortunately, this procedure could not be pursued profitably for ^{120}Sn because the unknown levels were only very weakly excited.

Since the present experimental program was begun the results of several other experimental studies of the nickel isotopes have become available. Elastic cross-section data at 18.6 MeV have been published by Eccles et al.[4]) and polarization data at 16.5 and 18.6 MeV have been obtained by Darriulat et al.[5,6]). Eccles et al. also measured the inelastic cross sections for scattering to the collective 2+ and 3- levels in several iron and nickel isotopes, but study of other levels was impossible with their energy resolution (200 keV). Inelastic scattering from Z = 28 isotopes has also been investigated by Roberson and Funsten[7]) at 17.5 MeV with good energy resolution but over a restricted angular range (30°-90°). The details of the present experimental procedure are described in section 2 and the results are described in section 3.

Before the current theories of inelastic scattering can be applied, the elastic scattering data must be reduced to the form of an optical model potential. Of the relevant optical model analyses made to date only that of Kossanyi-Demay et al.[6]) at 18.6 MeV used cross-section data (from ref. 4) obtained with separated isotope targets. The analyses of Baugh et al.[3,8]) at 17.8 MeV used the cross-section data of Dayton and Schrank[9]) in which targets of the natural elements were used. For this reason it was considered of value to repeat the analysis of the 17.8-MeV polarization data using our cross-section data for the nickel isotopes. No polarization data in the present energy region is currently available for ^{120}Sn. Using the potentials found in this analysis, DWBA calculations were carried out. For the collective 2+ and 3- levels a comparison was made between the results of using real and complex interaction potentials in these calculations, and the sensitivity to the particular choice of optical model potential was investigated. The results of this work are described in section 4.

The α-particle elastic scattering data were also analyzed in terms of the optical model. DWBA calculations were then made for each excited state and the quality of the fit to the data was the basis on which the spin assignments were made. This analysis is described in section 5.

Finally, in section 6, a comparison is made between the results of the proton and α-particle work and further tentative assignments are made. It is relevant to note that sometimes even the fact that a level is not excited at all in α-particle scattering can be combined with other experimental evidence to result in quite strong unique assignments.

2. Experimental Technique

The Berkeley 88-inch variable energy cyclotron was used as the source of bombarding particles (17.8-MeV protons or 50-MeV α particles). Much of the experimental arrangement has been described elsewhere[10]. The targets* consisted of isotopically enriched ^{58}Ni (99.95%), ^{60}Ni (98.21%), and ^{120}Sn (98.39%). These targets were used in the form of self-supporting evaporated metallic foils having surface densities of about 350 $\mu g/cm^2$, these densities being determined by weighing (to an estimated accuracy of about ±7%).

The particle beam was initially momentum analyzed by passage through a 0.15-cm slit placed behind a 57° magnet and was then focused (with no further

---

*Obtained from Stable Isotopes Division, Oak Ridge National Laboratory, Oak Ridge, Tennessee.

collimation) at the target position where it formed a beam spot about 0.3-cm high and 0.15-cm wide. The beam was finally collected in a magnetically shielded Faraday cup. The scattered particles were stopped in cooled lithium-drifted silicon detectors, 0.3-cm thick for the proton work and 0.15-cm thick for the α-particle work. Two detectors spaced 20° apart were used for the proton work but four detectors spaced 2° apart were used for the α-particle work where the angular distributions have considerable structure. The overall angular resolution of these detectors was about $\pm 0.25^{\circ}$. A separate silicon detector, set at a fixed scattering angle of 20°, was used throughout for monitoring purposes.

Pulses from the silicon detectors were amplified by charge sensitive pre-amplifiers placed within the vacuum system of the scattering chamber. After further amplification the pulses were routed into different quadrants of a Nuclear Data 4096 channel pulse-height analyzer. At the end of each cycle of data taking, determined by the collection of a pre-set charge in the Faraday cup charge integrator, the pulse-height spectra were transferred to a PDP 5 computer which plotted the spectra and also stored them on magnetic tape for further analysis at a later time.

Clearly resolved peaks in the experimental spectra could be analyzed immediately by using the light-pen facility of the PDP 5 computer, but where the levels were not clearly resolved it was necessary to use a least-squares routine[11]) which fitted gaussian shaped peaks to the levels of interest. This final data reduction was performed using the Lawrence Radiation Laboratory IBM 7094 computer. Little uncertainty in the results was introduced by the use of this fitting technique even though each peak did not possess a true gaussian shape and had a low energy tail containing about 3% of the total counts

in the peak. This tail was mainly due to a low energy component in the beam resulting from slit scattering at the analyzing magnet slit.

The relative errors were generally ±3% for the elastic scattering and between 4% and 25% for the inelastic levels depending upon their relative intensities and excitation energies. For the weaker levels background subtractions and statistics were the limiting factor, but in the case of peaks not clearly resolved there was also some uncertainty involved in the use of the fitting program. For the strongest peaks the statistical errors were negligible and the quoted errors reflect more the reproducibility of the data within a run (consisting typically of five 8-hour shifts). Impurity peaks were readily distinguished by their kinematic behavior with scattering angle; only carbon and oxygen were present in significant quantity. The presence of such impurities resulted in a loss of cross-section data for various energy levels at particular angles. Beam energies were measured by determining the range in aluminum and using range-energy tables[12]) and were checked by use of the scattering kinematics.

3. Experimental Results

Typical energy spectra for the three proton experiments and the single α-particle experiment are presented in figs. 1-4. These spectra are shown on logarithmic intensity scales and the energy scales are different in each case.

The energy level schemes are also shown in figs. 1-4. The scheme for ^{58}Ni is mostly that quoted by Swenson and Mohindra[13]); the spin and parity assignments for this nucleus will be discussed later. For ^{60}Ni the energies are the MIT values quoted by Matsuda[14]) and the spin and parity assignments

are as given by Mohindra and Van Patter[15]). For ^{120}Sn the energies are those given by Allen et al.[16]) and the spin and parity assignments are as discussed by them together with results obtained from the decay of ^{120}Sb[17]). For ^{58}Ni and ^{120}Sn the levels marked by an asterisk appear not to have been reported previously.

3.1. PROTON SCATTERING

The proton elastic scattering angular distributions are shown in figs. 5-7, where the results are displayed as ratios to the Rutherford cross sections.

^{58}Ni. The ^{58}Ni proton data were taken at an energy of 17.69±0.05 MeV and with an energy resolution (FWHM) of about 45 keV. Angular distributions were obtained for most of the low-lying levels (listed in table 4), the exceptions including the levels at 3.524 and 3.588 MeV which were only weakly excited, the doublets at about 4.9 and 5.1 MeV, and the group of levels (at least four) at about 5.45 MeV. The collective 3- level at 4.472 MeV is seen to be closely surrounded by several levels which are not all strongly excited. Of these levels reliable angular distributions could only be obtained for the 4.405- and 4.472-MeV levels. The experimental cross-section data are displayed in fig. 8, where the various levels have been grouped according to level spin as determined from the α-particle scattering measurements.

^{60}Ni. The ^{60}Ni data were taken at 17.91±0.05 MeV with a resolution of 30 keV. The 3.587- and 3.886-MeV levels were only weakly excited, and the 3.184- and 3.191-MeV levels appeared as an unresolved doublet. From figs. 1 and 2 it can be seen immediately that the majority of levels in ^{60}Ni are considerably less strongly excited than in ^{58}Ni. The level spacings are also smaller (note

the different energy scales). The angular distributions for the six most strongly excited levels are given in fig. 9. The remaining levels were isotropic (to within the fairly large statistical errors) and possessed differential cross sections in the range between 0.01 to 0.10 mb/sr.

^{120}Sn. The ^{120}Sn data were taken at 17.79±0.05 MeV with a resolution of 25 keV. The angular distributions for the most strongly excited states are shown in fig. 10. The levels at 1.872 and 2.088 MeV were almost isotropic at 0.01 to 0.02 mb/sr. No inelastic scattering data were obtained for angles forward of 45° owing to the very strong elastic scattering.

3.2. ALPHA-PARTICLE SCATTERING

^{58}Ni. The ^{58}Ni α-particle data were taken at 50.2±0.1 MeV with an energy resolution of about 80 keV. A restricted angular range (10°-65°) was studied as it is only necessary to obtain the positions of the first few diffraction maxima in order to determine the phase relationships between the various excited states. The very small angle scattering is of particular value but coulomb elastic scattering prevented much useful data being obtained for angles below 15°. Results of the α-scattering work are shown in fig. 11. Several levels were too weakly excited for useful data to be extracted; these levels are noted in table 4. The 5.07- and 5.10-MeV levels were not resolved, although both were strongly excited.

3.3. GENERAL

Where comparison between our proton data and that obtained by other workers is possible the agreement is found to be good. The elastic scattering data are

sensitive to the precise beam energies but there are no obvious systematic differences from the data of Dayton and Schrank[9]) or of Eccles et al.[4]). The inelastic scattering data for the 2+ and 3- levels in the nickel isotopes agree very well with those of Eccles et al. Agreement with the data of Roberson et al.[7]) is also good, within the somewhat limited statistics, and over the restricted angular range for which comparison is possible.

Elastic and inelastic scattering of α particles from ^{58}Ni have previously been studied at several energies[18,19]) but only a few excited states were considered and the energy resolution was poor.

4. Analysis of the Proton Scattering Data

4.1. THE OPTICAL MODEL

The optical model potential used in the present work took the form

$$V(r) = V_c(r) - V\left(\frac{1}{1+e^{x}}\right) - i\left(W - 4\,W_1\,a_w\,\frac{d}{dr}\right)\left(\frac{1}{1+e^{x_w}}\right) + \left(\frac{\hbar}{m_\pi c}\right)^2 (V_s + i W_s)\,\frac{1}{r}\,\frac{d}{dr}\left(\frac{1}{1+e^{x_s}}\right)\underline{\sigma}\cdot\underline{l}$$

where $x = (r-R_v)/(a_v)$, $x_w = (r-R_w)/(a_w)$, $x_s = (r-R_s)/(a_s)$, with $R_v = r_v A^{1/3}$, etc. The coulomb potential was assumed to have the form for a uniformly charged sphere

$$V_c(r) = \frac{Z e^2}{2 R_c}\left(3 - \frac{r^2}{R_c^2}\right), \quad r \le R_c$$

$$= \frac{Z e^2}{r}, \quad r > R_c$$

where $R_c = r_c A^{1/3}$. The optical model predictions for both cross-section $\sigma(\theta)$ and polarization $P(\theta)$ are insensitive to the value of r_c; the value $r_c = 1.25$ fm was assumed.

The optimum values for the optical model parameters were obtained using a modified version of the search code SEEK[20]. The parameters were varied so as to minimize the quantity $\chi^2 = \chi^2_\sigma + \chi^2_\pi$ where

$$\chi^2_\sigma = \sum_{i=1}^{N_\sigma} \left| \frac{\lambda \sigma_{th}(\theta_i) - \sigma_{exp}(\theta_i)}{\Delta\sigma(\theta_i)} \right|^2$$

$$\text{and} \quad \chi^2_\pi = \sum_{i=1}^{N_\pi} \left| \frac{P_{th}(\theta_i) - P_{exp}(\theta_i)}{\Delta P(\theta_i)} \right|^2 .$$

Because the overall normalization of the cross-section data was not precisely determined, the normalization factor λ was adjusted so as to optimize the fit to the data by satisfying the equation $(\partial \chi^2_\sigma)/(\partial\lambda) = 0$. No similar renormalization was used for the polarization data, although it will be seen later that such a procedure might have been desirable.

The experimental errors used in the evaluation of χ^2 were ±3% for the $\sigma(\theta)$ data. For the $P(\theta)$ data the measurements of Baugh et al.[3]) were used, the statistical errors quoted by them being increased in accordance with a later analysis of Baugh, Griffith, and Roman[8]) to make allowance for inelastic contamination and angular resolution effects.

The recent analysis of Kossanyi-Demay et al.[6]), Baugh et al.[8]), Boschitz[21]), Perey[22]), Greenlees and Pyle[23]), and Rosen et al.[24]) have demonstrated that the average parameters obtained by Perey[25]) in an extensive analysis of cross-section data need revision if polarization data are also to be

fitted. The modifications concern mainly the spin-orbit parameters, which are conveniently summarized by Boschitz[21]) for the 18.5-to 20.5-MeV range as $v_s = 5.5\pm0.5$ MeV, $a_s = 0.55\pm0.05$ fm, $r_s = 1.12\pm0.05$ fm. For the present analysis the initial values for the central part of the potential were taken from the results of Baugh et al.[8]). No satisfactory method of searching for a best solution was found and our final parameter sets were eventually obtained by fitting the $\sigma(\theta)$ and $P(\theta)$ data for ^{60}Ni separately and using the averaged parameters as starting values for the combined analysis. Perversely, this procedure was unsatisfactory for ^{58}Ni, for which the best fit was obtained starting directly from the final parameters of the ^{60}Ni solution. The final parameter sets are given in table 1.

In agreement with refs. 6, 21, and 22, where a_s was treated as a separate parameter, we found $a_s \simeq a_w \simeq 0.5$ fm. In the other analyses a_s was set equal to a_v. Further, with a_s separately adjusted we found r_s to be no longer sensitively determined and $r_s = r_v = 1.25$ fm would have been acceptable. Combinations of volume and surface absorption were tried but pure surface absorption gave the best results. The central radius r_v was not treated as a search variable but it was found that equally good solutions existed for $1.15 \text{ fm} \leq r_v \leq 1.30$ fm. The fits to the data were not improved by changing W_s from its expected value of zero.

The diffuseness parameter a_v was found to be much greater than the value 0.65 fm proposed by Perey. It is this feature which is responsible for the large values predicted for the reaction cross-sections (σ_R). Pollock and Schrank[26]) have determined $\sigma_R = 898\pm53$ mb for natural nickel at 16.4 MeV. Further measurements at 17 MeV have been made by Cole et al.[27]) in which the

appreciably larger result $\sigma_R = 1015 \pm 32$ mb was obtained as an average of two experiments (which gave the same result). These results are essentially attributable to ^{58}Ni and the cross section for ^{60}Ni could well be 70 mb greater[28]). No attempt was made to force a fit to these data. In the present context it is interesting to note the situation which exists in proton scattering in the 150- to 180-MeV region, recently discussed by Elton[29]). At these high energies a fit to the differential cross-section data forces the imaginary part W(r) of the Saxon-Woods potential to extend to larger radii than the real part V(r). This feature results in reaction cross-section predictions which are too large. To obtain a simultaneous fit to both $\sigma(\theta)$ and σ_R data Elton demonstrated the apparent necessity for V(r) to become repulsive in the central region of the nucleus. It is tempting to consider that a similar feature could improve the present situation at 18 MeV.

Our final parameter sets are rather different from those of Kossanyi-Demay et al.[6]), in whose analyses the average parameters of Perey[25]) were retained as far as possible. That some difference in parameters should necessarily occur is made clear by a comparison of the polarization data for the nickel isotopes at 16.5, 17.8, and 18.6 MeV obtained by the Saclay[6]) and Birmingham[3]) groups. Although the two groups claim normalization of their data to the same polarimeter calibration[30]), the Saclay data were larger by a factor of about 1.3 than the Birmingham data. The reason for this discrepancy is not obvious.

The importance of adjusting the spin-orbit geometry factors separately is demonstrated by the larger values of χ^2 (see table 1) obtained when the $\sigma(\theta)$ and $P(\theta)$ data were analyzed with the applied constraints $a_s = a_v$ and $r_s = r_v$.

In order to gain some idea of the importance of the choice of the optical model parameters on the DWBA calculations we also chose to fit the cross-section data alone, with V_s heated as an adjustable parameter. The ^{120}Sn data were included in this analysis. In figs. 5-7 the optical model predictions for the potentials giving the best fit to both cross-section and polarization data are compared with predictions for the potentials which fit only the cross-section data.

4.2. DWBA ANALYSES

The inelastic scattering to the "collective" vibrational 2+ and 3- levels is assumed to be caused by a direct reaction. For these calculations the DWBA computer code JULIE was used[31,32]). For orientation purposes a very brief sketch of the calculation is given here. Using the conventional nomenclature, the DWBA theory gives the inelastic scattering differential cross section as

$$d\sigma/d\Omega = (\mu/2\pi\hbar^2)^2 (k_f/k_i) \sum_{Av.} |T_{fi}|^2$$

where the transition amplitude is

$$T_{fi} = \int d\underline{r}\ \chi_f^{(-)*}(\underline{k}_f, \underline{r}) \langle \nu_f | V | \nu_i \rangle \chi_i^{(+)}(\underline{k}_i, \underline{r}).$$

The $\chi(k,r)$ are the distorted waves describing the elastic scattering of the particle by the nucleus before and after the inelastic transition; these distorted waves are generated from the optical model potential. After application of the Wigner-Eckart theorem to the matrix element contained in T_{fi} a reduced matrix element is obtained which, within the framework of the collective model, is a product of the deformation parameter β_L and the radial derivative of the optical

model potential which describes the elastic scattering. Thus, β_L is the only quantity appearing in the calculation which is not pre-determined.

The results of the DWBA calculations for the 2+ and 3- collective levels are shown in figs. 8-10 and the values for β_L are presented in table 2, together with the results of other workers. These calculations were made for both real and complex deformed potentials. It is now recognized that the calculation in which the complex deformed potential is used generally gives the better fit to experimental data and we demonstrate in section 5.2 that certain ambiguities present in the analysis of the α-particle data can only be resolved if the complex interaction form is used. Figs. 8-10 show that the magnitudes of the cross sections for the collective levels are little affected by the change from real to complex form for the deformed potential, but the complex form does produce the better fit to the data.

In our calculations the spin-orbit part of the potential could not be deformed; inasmuch as $V_s^2/W^2 \lesssim 0.3$ the inclusion of this term would be expected to produce even less effect than the change from real to complex form factors. At higher energies deformation of the spin-orbit term can be important[33]).

The optical model potentials used for the nickel DWBA calculations displayed in figs. 8-10 were those giving the best fit to both cross-section and polarization data. Calculations were also made with the potentials obtained by fitting only the cross-section data; it was found that although the shapes of the calculated angular distributions were very similar for the two potentials, the resulting values for β_2 were significantly different (see table 2). We would naturally expect that the correct choice of potential to be that which fits both cross-section and polarization data. This choice is supported by the agreement shown in table 2 with the β_2 values obtained by other methods.

The calculations discussed above included coulomb excitation as a possible excitation mode. In table 2 the values given within parentheses were obtained with the coulomb excitation mechanism neglected. It can be seen that the sensitivity of β_2 to the optical potentials obtains only when the coulomb excitation mechanism is included. The present sensitivity to the optical potential is due to the coulomb excitation amplitude interfering destructively with the nuclear amplitude, this effect being most serious for small angles (up to the first maximum). Thereafter, it acts only as a scaling factor to reduce the nickel cross sections by about 10% for the 2+ levels and 5% for the 3- levels. This sensitivity to the inclusion of coulomb excitation would be minimized by fitting the calculations to the data by using the least-squares method, rather than normalizing to the first maximum as we have done (following the customary procedure). However, the theoretical fit to the data is not sufficiently good for the correct fitting procedure to be followed and, moreover, the collective model calculations are expected[34]) to apply best for the forward angle scattering. From the above discussion it will be realized that our final values for β_L have associated uncertainties of at least ±10%.

It is well-known that the optical model potential is energy dependent, but in the present calculations the distorted waves for the outgoing channel were generated from the same potential as used for the incoming channel and the interaction. We found the results of the DWBA calculations to be quite insensitive to this simplification by performing calculations for the nickel isotopes in which the outgoing distorted waves were generated from the potentials obtained by Lind et al.[35]) in an analysis of both cross-section and polarization data at 14.5 MeV.

As shown in table 2, the values obtained by Eccles et al.[4]) for β_L from DWBA calculations are significantly higher than our results, despite the apparent similarity between both the experimental data and the calculated angular distribution shapes. This comparison should be made to our set of parameters obtained from the real interaction calculations using the optical model potential which fitted the cross-section data only and which included the coulomb excitation mechanism. It is interesting to note that the shapes of the angular distributions calculated by Eccles et al. for the 2+ states using a coupled-channels code are very similar to our results using the complex interaction form-factor DWBA calculation. (The values obtained for β_2 are also smaller than those obtained from their DWBA calculation.) This confirms their speculation that the difference between their DWBA and coupled-channels calculations lies mainly in the fact that only the latter included a complex form factor. Consequently, we conclude that the magnitude of the deformation parameter is small enough that the DWBA calculation represents a valid approximation in the present case.

The calculations of Roberson and Funsten[7]) included only the real interaction form factor. Moreover, they used Perey's averaged optical model potentials but excluded the spin-orbit term from the calculation of the distorted waves. These two approximations make very little difference to the shape of the angular distributions in the forward hemisphere. In fact, the neglect of the spin-orbit potential in the elastic scattering channels has no greater effect on the complete angular distribution than does neglect of the imaginary part of the interaction potential. The excellent agreement of Roberson and Funsten's values with our final preferred set is presumably fortuitous.

Also shown in table 2 are the values for β_L obtained by Fricke and Satchler[36]) in an analysis of proton scattering at 40 MeV, the averaged values obtained from high energy electron scattering and coulomb excitation methods[37]), and finally the values obtained from the analysis of our (α,α') work on ^{58}Ni. As pointed out by Blair[38]) the important quantity determined in the DWBA calculations is the product $\beta_L R$, where R is the interaction radius, rather than β_L alone. Consequently, the results quoted here have been corrected to correspond to a radius $R = 1.25\ A^{1/3}$ fm. The agreement between our (p,p') and (α,α') work is excellent. The different methods for determining β_L agree to about ±10%, which is within the experimental errors for most determinations.

DWBA calculations using the collective model form factor were also made for levels other than the strong collective levels. The results of these calculations for such levels clearly needs some justification. Use of the DWBA (in first order) requires that the levels should be excited in a direct single-excitation process. Such levels should be excited more strongly than those for which a more complicated mechanism is involved. Our experimental results are consequently biased in favor of levels excited directly because angular distributions were only obtained for the strongest levels. The collective model form factors are known to give good results for <u>α-particle</u> scattering because, owing to the strong absorption, the angular distributions are characterized mainly by the angular momentum transfer and the form factors serve mainly to give an overall scaling factor[1]). Thus we certainly expect spin assignments from α-particle scattering to be reliable but the derived deformation parameters may be peculiar to α-particle scattering. In proton scattering, by contrast, the angular distributions are sensitive to the nature of the form factors

and there is no obvious reason for the collective model to be applicable other than for the strongest ("collective") levels. However, when the results of the collective model calculations are compared with the more appropriate calculations which assume single-particle excitations in nuclei where the shell-model wave functions are known fairly well it is found that the two sets of calculated angular distributions compare rather well, although the absolute scales may differ considerably. This result is expected to hold for the "collective" levels (see ref. 4) but was also found to hold for some weaker levels in ^{52}Cr by Funsten et al.[40]) and for the Zr isotopes by Gray et al.[41]) and Stautburg and Kraushaar[42]) for 19-MeV protons. Thus we may expect our collective model calculations to reproduce the shape of the angular distributions and so to provide a possible method of making spin assignments from proton scattering. In fact we found that this was indeed possible for the 4+ levels in ^{58}Ni. The β_4 values, however, probably constitute little more than a convenient method of parametrizing the data. It is of interest, however, to compare β_L values derived from fitting the non-collective levels excited in proton scattering with those obtained from α-particle scattering. This is done in table 4, where the agreement is found to be surprisingly good.

5. Analysis of the α-Particle Scattering Data

5.1. OPTICAL MODEL

In the analysis of the α-particle scattering from ^{58}Ni the optical model potential was assumed to have the customary volume imaginary part. As only a restricted angular range was covered the further restriction of equal geometric parameters for real and imaginary parts of the potential was assumed—

thus, there were only four adjustable parameters. As is very well-known[43]), α-particle scattering does not yield a unique optical potential, but rather a set of potentials. This is illustrated in table 3 where five acceptable sets of parameters are given. The quantity χ^2/point was calculated assuming relative cross-section errors of ±5%. The quality of the fit is shown in fig. 11(a), where the ratio of cross section to the Rutherford cross section is presented. The several sets of parameters give very similar predictions.

5.2. DWBA ANALYSES

The DWBA analysis of 43-MeV α particles scattered from ^{58}Ni has been described in detail by Bassell et al.[39]). We assume here that both real and imaginary parts of the optical potential should be deformed; in the present case inclusion of the imaginary part serves only to change the overall scale factor (β^2). The effect of including coulomb excitation as a possible excitation mode was found to be negligible over the angular range for which we have data. The optical model potential used for the following analysis was that with V ≈ 70 MeV as this gave, marginally, the best fit to the elastic scattering data. However, calculations were made for the collective 2+ level using each of the five potentials in turn. The resulting angular distributions were almost identical but the magnitudes of the cross sections were slightly different. For each potential the values for β were obtained from the best fit of the DWBA curves to the several maxima of the experimental cross sections; these values varied between 0.164 and 0.176. After correction for the differing interaction radii through the relationship

$$\beta = \beta_R R/(1.25\ A^{1/3})$$

the values obtained for β were in the range 0.212 to 0.196, in good agreement with the proton scattering result. For a real interaction form factor this variation would have been from 0.25 to 0.20. Thus, for the complex interaction calculation the particular choice of optical potential is unimportant.

The angular distributions for the elastic and inelastic levels have already been presented in fig. 11(a,b,c). These figures also show the results of the DWBA calculations, each curve representing the particular angular momentum transfer which best fits the data.

For the strongly excited levels on 1.456(2+), 3.615(4+), 4.472(3-), and 4.75 MeV (4+) the DWBA curves based on the one-phonon form factor produce excellent fits to the data leaving no doubt as to the level spins nor to the direct one-step nature of the excitation process. The 1.456-and 4.472-MeV levels are, of course, the well-known 2+ and 3- collective levels. The fits to the remaining levels are not so definite and will be considered in order of excitation energy.

The 2.458-MeV level has already been given a 4+ assignment[45,46]; the DWBA curve for L = 4 indeed gives the best fit, which is good at small angles but which moves gradually out of phase with increasing angle. This behavior is interpreted by assuming that a multiple excitation process is competing with the direct excitation mechanism at the present energy. It has been shown[44] that a level formed by such a double excitation process (in this case two quadrupole phonons are involved) should be out of phase with the distribution

expected for a direct excitation. Such a double excitation mechanism would be most important at large angles because the overall slope of the angular distribution shows a distinctly less sharp fall with angle for the double-excitation process than for the direct process. Double excitation of the first 4+ level in medium weight nuclides has been discussed previously[18,19,47]. Thus, our results may be interpreted as showing this 4+ level to be a combination of one hexadecapole phonon and two quadrupole phonons.

The 2.773-MeV level was originally given a tentative 0+ assignment[48] but Henrickson et al.[45] now regard this as most unlikely. A spin of 2 or 3 is indicated by (p,p') work[13] in the compound nucleus energy region, between 9 and 10 MeV. Our (α,α') angular distribution looks peculiar, but at large angles is in phase with the elastic scattering which would indicate negative parity. As a negative parity state at such a low excitation is most unlikely, and as unnatural parity states are unlikely to be strongly excited in α-particle scattering[49], we conclude that this is probably a 2+ state formed by double excitation. This accounts both for the reversed phase and the peculiar small angle behavior. It also provides support for the collective two-phonon description of the second 2+ state.

The 2.900-and 2.940-MeV levels were not resolved in the (α,α') work, and were only weakly excited. The 2.900-MeV level has been assigned spin 1 in low energy (p,p') scattering[13]. The weak excitation by α particles implies positive parity. The 2.940-MeV level could be the missing 0+ level of the two-phonon triplet (which the collective model would lead us to expect at an excitation energy of double that of the first 2+ level)—indeed, it now seems

to be the only candidate for this assignment. This would be in agreement with the weak excitation by α particles and is strongly supported, if not confirmed, by the proton work (see section 6).

The 3.035-and 3.260-MeV levels have distributions characteristic of spin 2+. This is in agreement with previous assignments (see table 4). However, the excitations are clearly more complicated than the direct single excitation which is appropriate for the collective 2+ level. The 3.414-MeV level is very weakly excited. It has been given [13] a spin of 2 or 3 from the low energy (p,p') work. The assignment of $(J\pi) = 3+$ is therefore preferred. The 3.524-MeV level is best fit assuming a 4+ assignment in agreement with other work[46,48]. The 3.588-MeV level has been assigned[45] a spin 1 or 2 and the very weak α excitation is consistent with $J\pi = 1+$. The 3.773-MeV level has been assigned spin 3, the weak excitation by α particles implies positive parity. The 3.895-MeV level clearly has $J\pi = 2+$.

The 4.103-MeV level has been assigned[13,45] spin 2. Our (α,α') angular distribution is peculiar in that it completely lacks the usual oscillatory behavior. The implication is that this level in fact consists of a very close doublet, or else the excitation mechanism is particularly complicated. Finally, both 4.405-and 5.59-MeV levels were best fitted by the $L = 4$ calculations.

The above comments and conclusions are summarized in table 4. The spin and parity assignments given in fig. 1 were based upon a consideration of the data contained in this table. Also contained in table 4 are the values for β_L (for $R = 1.25\ A^{1/3}$ fm) deduced from the DWBA calculations. To simplify comparison with results from different experiments we have also included the ratios of the electromagnetic reduced matrix element to its single-particle value

$B(E\lambda,\lambda\rightarrow 0)/B(E\lambda,\lambda\rightarrow 0)_{sp}$. This ratio is determined using the formulae

$$B(E\lambda,\lambda\rightarrow 0) = \left(\frac{3\,Z\,e\,R^{\lambda-1}}{4\pi}\right)^2 \frac{(\beta_\lambda R)^2}{2\lambda+1}$$

and

$$B(E\lambda,\lambda\rightarrow 0)_{S.P.} = \frac{1}{4\pi}\left(\frac{3\,e\,R^{\lambda}}{3+\lambda}\right)^2$$

where $R = 1.20\ A^{1/3}$ fm, as usually used for electromagnetic work. Unfortunately, very few measurements have been made of these transition strengths except for the first 2+ level, for which good agreement has already been demonstrated. We show the results of the electron scattering work of Crannell et al.[50] in table 4. The agreement between the results of the two very different experimental methods is encouraging.

6. Discussion

The most important preliminary to the theoretical description of the proton inelastic scattering results is the determination of spin and parity assignments. It is therefore of interest to examine the proton scattering angular distributions to see whether it is possible to make new assignments or, for ^{58}Ni, at least check assignments made from the (α,α') work. As discussed in section 4.2, the collective model DWBA calculations may be expected to be of some value in such work.

6.1. ^{58}Ni

^{58}Ni was investigated most thoroughly because the low-lying excited states are quite strongly excited both by (p,p') and (α,α') scattering and the experimental energy resolution was adequate to resolve the majority of the levels. In fig. 8 the various angular distributions are grouped together according to the spins as determined from the (α,α') work. The 2+ levels show quite distinct similarities. The two levels at 3.414 and 3.773 MeV (tentatively given 3+ assignments) possess nearly identical angular distributions and the group of 4+ levels are all very similar. As displayed in the figure the grouping appears quite natural and consequently provides strong supporting evidence for the assignments.

DWBA calculations were made for the noncollective 2+ and 4+ levels. The only 2+ level fitted well was that at 3.895 MeV but all the 4+ distributions bore a considerable resemblance to the calculations, the poorest fit being for the first (2.458-MeV) level. The values for β obtained from these calculations are presented in table 4 where they can be seen to agree very well with the results of the (α,α') work. In view of our earlier comments regarding extracting β values from the weak levels this agreement should be regarded as very surprising, indicating possibly that the present DWBA calculation approach based on the one-phonon form factor has greater validity than is expected. However, although the present calculations fit the data quite well it would clearly not be safe to make spin assignments directly from such (p,p') work alone.

The results for the 2.900- and 2.940-MeV levels are of poor quality because these levels are only weakly excited and were barely resolved. However, study of even these data permits a very strong assignment of spin 0 to the 2.940-MeV level to be made. Two pieces of evidence are available for this

purpose. The first, and strongest, is the similarity between the angular distributions for the 2.940-MeV level in ^{58}Ni and the 2.286-MeV level in ^{60}Ni, which is a known 0+ level. Both distributions show a deep minimum at 90°, a feature not shared by any other levels. The second piece of evidence is rather tenuous and depends on the observation that the 2.90-and 2.94-MeV levels are symmetric about 90°, which indicates that the main excitation mechanism may be through the compound nucleus. Assuming this to be the case, we can compare the ratios of the integrated cross sections with the (2J+1) rule. We find these cross sections for the 2.90-and 2.94-MeV levels to be in the ratio (1.9±0.9):1. Accepting the spin 1 assignment of Swenson and Mohindra[13]) for the 2.90-MeV level leads to the suggestion of spin 0 for the 2.94-MeV level. That this ratio is reduced from the simple compound nucleus value of 3:1 is to be expected because the collective model two-phonon description of the first-excited 0+ state would lead to a cross section weakly enhanced through a double-excitation process over the compound nucleus value. No such simple enhancement for the spin-1 level is expected. The alternative conclusion (see ref. 13) that the 2.94-MeV level has a high spin (~6) which would also yield a compound nucleus cross section of the right magnitude (after allowance has been made for the centrifugal barrier penetrability) can be excluded because it would not give an angular distribution which displayed a minimum at 90°.

6.2. ^{60}Ni

As would be expected, the ^{60}Ni(p,p') results are very similar to those for corresponding levels in ^{58}Ni. Only the collective 2+ and 3- levels were well described by our use of the one-phonon form factors in the DWBA calculations. The other levels were not well represented and hence presumably have different form factors and/or receive important contributions from several-step scattering processes.

6.3. ^{120}Sn

For ^{120}Sn the collective 2+ and 3- levels were fitted quite well by the DWBA calculations. However, as for the nickel isotopes the fit to the first 4+ level is not good ($\beta_4 \approx 0.03$) but the 2.272-MeV level, which is presumably the 5- level discussed by Bolotin et al.[17]), is fitted very well by the L = 5 calculation (with $\beta_5 = 0.05$). Spin assignments have not previously been made for the remaining levels. The angular distributions for the 2.455-,2.67-, 3.06- and 3.17-MeV levels are all very similar and are fitted adequately by the L = 4 calculations (with β_4 values 0.08, 0.04, 0.04, 0.07). The 3.45-MeV level is best fit by L = 3 but the quality of the fit is poor. It will be interesting to see if these tentative assignments can be confirmed by other experimental techniques.

7. Conclusion

The inelastic scattering of 17.8-MeV protons from a number of levels in ^{58,60}Ni and ^{120}Sn has been studied. As expected, the scattering from the known collective levels has been found to be fitted quite well by the DWBA calculations. However, it was shown that care should be taken in these calculations to use optical model potentials which fits both elastic scattering cross-section and polarization data. When this was done the resulting values for the deformation parameter agreed with values derived from other methods. In particular good agreement with values obtained from the (α,α') work was obtained.

The ^{58}Ni(p,p') data was examined closely and it was found that the angular distributions for levels of the same spin displayed quite similar

shapes. The collective model DWBA calculations were also compared with the non-collective levels in all three nuclei and it was found that many of these levels were fitted quite well. A possible reason for the success of these collective model DWBA calculations lies in the fact that a relatively low proton energy was chosen with the result that the long wave length of the incident protons averages over the details of the interaction form factor whereas at higher energies these details would be of importance. The calculations of Glendenning and Veneroni[1]) show this effect in the comparison of the cross section for 11- and 40-MeV protons.

The combination of the present results for ^{58}Ni of both (p,p') and (α,α') experiments with other work has yielded strong spin and parity assignments for the majority of levels below 5-MeV excitation. It is interesting to note that levels have been identified in ^{58}Ni which may be associated with the expected collective two-phonon triplet of 0+, 2+, 4+ levels. This feature is of importance for the microscopic description of the inelastic scattering using the two quasiparticle description of Arvieu et al.[2]) because such a description can only describe single phonon collective levels, four quasiparticles being required to describe two-phonon levels. Preliminary results of the calculations of Glendenning using this model have already been published[1]) and comparisons* with the present data have also been given[51,52]).

Acknowledgments

The authors would like to acknowledge the assistance of the operating crew of the 88-inch cyclotron and are grateful to Claude Ellsworth for preparing the targets.

*In ref. 51 the 2.773 MeV level in ^{58}Ni was incorrectly assumed to possess (Jπ)=0+.

References

1) N. K. Glendenning and M. Veneroni, Phys. Rev. 144 (1966) 839

2) R. Arvieu, E. Salusti, and M. Veneroni, Phys. Letters 8 (1964) 334

3) D. J. Baugh, G. W. Greenlees, J. S. Lilley, and S. Roman, Nucl. Phys. 65 (1965) 33

4) S. F. Eccles, H. F. Lutz, and V. A. Madsen, Phys. Rev. 141 (1966) 1067

5) P. Darriulat, J. M. Fowler, R. De Swiniarski, and J. Thirion, Proceedings of Karlsruhe Conference on Polarization Phenomena of Nucleons (September 1965)

6) P. Kossanyi-Demay, R. De Swiniarski, and C. Glashausser, Nucl. Phys. (to be published)

7) N. R. Roberson and H. O. Funsten, Bull. Am. Phys. Soc. 9 (1964) 93 (and private communication)

8) D. J. Baugh, J. A. Griffith, and S. Roman, Nucl. Phys. 83 (1966) 481

9) I. E. Dayton and G. Schrank, Phys. Rev. 101 (1956) 1358

10) B. G. Harvey, E. J.-M. Rivet, A. Springer, J. R. Meriwether, W. B. Jones, J. H. Elliot, and P. Darriulat, Nucl. Phys. 52 (1964) 465

11) A. Springer, Lawrence Radiation Laboratory Report UCRL-11681 (1965)(unpublished)

12) C. Williamson and J. Boujot, Range Tables, CEA 2189, Saclay (1962)

13) L. W. Swenson and R. K. Mohindra, Phys. Rev. 150 (1966) 877

14) K. Matsuda, Nucl. Phys. 33 (1962) 536

15) R. K. Mohindra and D. M. Van Patter, Phys. Rev. 139 (1965) B274

16) D. L. Allen, B. H. Armitage, and Beryl A. Doran, Nucl. Phys. 66 (1965) 481

17) H. H. Bolotin, A. C. Li, and A. Schwarzschild, Phys. Rev. 124 (1961) 213

18) D. J. Horen, J. R. Meriwether, B. G. Harvey, A. Bussière de Nercy, and Jeannette Mahoney, Nucl. Phys. 72 (1965) 97

19) H. W. Broek, T. H. Braid, J. L. Yntema, and B. Zeidman, Phys. Rev. 126 (1962) 1514

20) M. A. Melkanoff, J. Raynal, and T. Sawada, UCLA Report No. 66-10 (January 1966)

21) E. Boschitz, Phys. Rev. Letters 17 (1966) 97

22) F. G. Perey, Proceedings Karlsruhe Conference on Polarization Phenomena of Nucleons (September 1965)

23) G. W. Greenlees and G. J. Pyle, Phys. Rev. 149 (1966) 836

24) L. Rosen, J. G. Beery, A. S. Goldhaber, and E. H. Auerbach, Ann. Phys. 34 (1965) 96

25) F. G. Perey, Phys. Rev. 131 (1963) 745

26) R. E. Pollock and G. Schrank, Phys. Rev. 140 (1965) B675

27) R. K. Cole, M. Q. Makino, D. G. Montague, and C. N. Waddell, Ann. Prog. Rep. USC-136-114 (October 1966)

28) J. F. Dicello, G. Igo, and M. L. Roush, Phys. Rev. 23 (1966) 685

29) L. R. B. Elton, Nucl. Phys. 89 (1966) 69

30) R. M. Craig, J. C. Dore, G. W. Greenlees, J. S. Lilley, and P. C. Rowe, Nucl. Instr. Methods 30 (1964) 268

31) R. H. Bassell, R. M. Drisko, and G. R. Satchler, Oak Ridge National Laboratory Report ORNL-3240 (1962)

32) G. R. Satchler, Nucl. Phys. 55 (1964) 1

33) M. P. Fricke, R. M. Drisko, R. H. Bassell, E. E. Gross, B. J. Morton, and A. Zucker, Phys. Rev. Letters 16 (1966) 746

34) W. T. Pinkston and G. R. Satchler, Nucl. Phys. 27 (1961) 270

35) D. A. Lind, H. G. Graetzer, D. Haegerty, and J. Kelly (private communication)

36) M. P. Fricke and G. R. Satchler, Phys. Rev. 139 (1965) B567

37) P. H. Stelson and L. Grodzins, Nuclear Data (Section A) 1 (1965) 21

38) J. S. Blair, "Proceedings of Conference on Direct Interactions and Nuclear Interaction Mechanisms," Ed. by E. Clementel and C. Villi (Gordon and Breach, Science Publishers Inc., New York, 1963) pp. 669

39) R. H. Bassell, G. R. Satchler, R. M. Drisko, and E. Rost, Phys. Rev. 128 (1962) 2693

40) H. O. Funsten, N. R. Roberson, and E. Rost, Phys. Rev. 134 (1964) B117

41) W. S. Gray, R. A. Kenefick, J. J. Kraushaar, and G. R. Satchler, Phys. Rev. 142 (1966) 735

42) M. M. Stautburg and J. J. Kraushaar, Phys. Rev. 151 (1966) 969

43) L. McFadden and G. R. Satchler, Nucl. Phys. 84 (1966) 177

44) N. Austern and J. S. Blair, Ann. Phys. 33 (1965) 15

45) P. F. Hinricksen, G. T. Wood, and S. M. Shafroth, Nucl. Phys. 81 (1966) 449

46) R. K. Jolly, E. K. Lin, and B. L. Cohen, Phys. Rev. 128 (1962) 2292

47) G. Bruge, J. C. Faivre, H. Farragi, G. Vallois, A. Bussière, and P. Roussell, Phys. Letters 22 (1960) 640

48) S. M. Shafroth, A. K. Sen Gupta, and G. T. Wood, Bull. Am. Phys. Soc. 9 (1964) 93

49) W. W. Eidson and J. G. Cramer, Phys. Rev. Letters 9 (1962) 497

50) H. Crannell, R. Helm, H. Kendall, J. Oeser, and M. Yearian, Phys. Rev. 123 (1961) 923

51) N. K. Glendenning, B. G. Harvey, D. L. Hendrie, O. N. Jarvis, and Jeannette Mahoney, Proceedings of International Conference on Nuclear Physics, Gatlinburg, Tennessee (September 1966)

52) N. K. Glendenning, Phys. Letters 21 (1966) 549

Table 1

Optical Model Parameters for Proton Scattering at about 17.8 MeV

	λ	V	a_v	r_v	W_1	a_w	r_w	V_s	a_s	r_s	σ_R(mb)	χ^2_σ/N_σ	χ^2_π/N_π
Ni^{58}	1.006	46.94	0.781	1.25	10.90	0.432	1.304	4.39	0.530	1.202	1078	21.9	9.8
Ni^{60}	0.984	46.45	0.846	1.25	11.90	0.465	1.279	5.48	0.502	1.253	1185	17.3	11.6
Ni^{58}	1.008	47.21	0.770	1.25	10.98	0.434	1.289	4.04	a_v	r_v	1072	28.4	19.5
Ni^{60}	0.978	47.42	0.843	1.25	12.60	0.448	1.282	4.74	a_v	r_v	1185	22.5	29.5
Ni^{58}	1.000	46.75	0.678	1.25	13.07	0.389	1.259	9.06	a_v	r_v	958	4.2	
Ni^{60}	1.000	46.59	0.754	1.25	14.19	0.422	1.261	8.89	a_v	r_v	1090	3.0	
Sn^{120}	1.000	50.70	0.665	1.25	13.22	0.556	1.230	7.40	a_v	r_v	1243	2.6	

Note: Potential depths are given in MeV, lengths in fm.

UCRL-17352

Table 2

Values of the deformation parameters for the collective levels derived from the present data compared with other results

Target	Jπ	Q(MeV)	1	2	3	4	5	6	7	8	9	10
			Complex		Real		18.6 MeV (p,p')		17.5 MeV	40 MeV	C.E.	50 MeV
			(σ+P)	σ	(σ+P)	σ	DWBA	C.C.	(p,p')	(p,p')		(α,α')
^{58}Ni	2+	-1.456	0.21(0.20)	0.24(0.20)	0.22(0.20)	0.25(0.22)	0.24	0.21	0.21	0.18	0.18±0.01	0.21
	3-	-4.472	0.16(0.15)	0.17(0.16)	0.15(0.15)	0.17(0.16)	0.19		0.15	0.18		0.15
^{60}Ni	2+	-1.332	0.21(0.20)	0.25(0.20)	0.22(0.195)	0.24(0.22)	0.30	0.26	0.21	0.21	0.20±0.01	
	3-	-4.038	0.17(0.17)	0.18(0.17)	0.15(0.145)	0.16(0.15)	0.22		0.17	0.16		
^{120}Sn	2+	-1.166		0.12(0.11)		0.13(0.12)					0.107±0.010	
	3-	-2.391		0.14(0.14)		0.14(0.14)						

Notes: Present (p,p') results are given in the first four columns. (σ+P) denotes results from optical model potential which fitted both cross-section and polarization data, etc. "Complex" and "Real" refer to the interaction form-factor. The first column contains our preferred (p,p') set. The values for β_L contained within parentheses were obtained without coulomb excitation as a possible excitation mode.

Columns 5 and 6 show the results of Eccles et al.[4]) using DWBA and coupled-channels calculations.

Columns 7 and 8 show the (p,p') results of Roberson and Funsten[7]) and of Fricke and Satchler[36]).

Column 9 gives the averaged results obtained in electron scattering and coulomb excitation work[37]).

Column 10 gives our (α,α') results.

The results quoted in columns 8-10 have been corrected to $R = 1.25\ A^{1/3}$ (see text).

Table 3

Optical Model Parameters for $^{58}Ni(\alpha,\alpha)$ at E_α = 50.2 MeV

	V	W	r_v	a_v	σ_R(mb)	χ^2/N
1	33.4	15.1	1.610	0.608	1600	5.5
2	69.7	19.1	1.508	0.584	1550	4.6
3	105.3	22.3	1.456	0.571	1533	5.5
4	144.5	25.4	1.417	0.563	1525	6.9
5	188.2	28.8	1.385	0.557	1519	8.4

Note: Potential depths are given in MeV, lengths in fm.

Table 4

Summary of Data on Spin and Parity Assignments for ^{58}Ni

Level (MeV)	(p,p'γ) ref. 45	(e,e') ref. 50	(p,p') ref. 13	(d,d') ref. 46	This work (α,α')	This work $\beta_L(\alpha,\alpha')$	This work $\beta_L(p,p')$	$B(E\lambda)/B(E\lambda)_{s.p.}$ (α,α') Present	$B(E\lambda)/B(E\lambda)_{s.p.}$ (e,e') ref. 50	Final Jπ values
5.59					4+	0.06 ±0.01	0.11±0.03	1.51		4+
5.45 (group)										
5.10					not res.					
5.07										
4.95										
4.90										
4.75					4+	0.08 ±0.01	0.11±0.03	2.2 ±0.6		4+
4.52+4.54					weak					
4.472		3-			3-	0.15 ±0.01	0.16±0.02	7.8 ±1.0	13.2±1.8	3-
4.444					weak					
4.405					4+	0.08 ±0.01	0.09±0.03	2.4 ±0.6		4+
4.383					weak					
4.347+4.352					weak					
4.291										
4.103	2	(2)								2
3.895		2			2+	0.035±0.005	0.04±0.01	0.4 ±0.1		2+
3.773		3			v. weak					3(+)
3.615					4+	0.050±0.005	0.08±0.03	0.9 ±0.2		4+
3.588	1,2				v. weak		weak			(1+)

(continued)

Table 4. (continued)

Level (MeV)	(p,p'γ) ref. 45	(e,e') ref. 50	(p,p') ref. 13	(d,d') ref. 46	This work (α,α')	This work $\beta_L(\alpha,\alpha')$	This work $\beta_L(p,p')$	$B(E\lambda)/B(E\lambda)_{s.p.}$ (α,α') Present	$B(E\lambda)/B(E\lambda)_{s.p.}$ (e,e') ref. 50	Final Jπ values
3.524		4+		4+	4+	0.035±0.005	weak	0.45±0.15	2.5±0.6	4+
3.414			2,3		v. weak					(3+)
3.260	2+	2+	2+	2+	2+	0.065±0.007		1.4 ±0.3	4.5±1.6	2+
3.035	low J			2+	2+	0.053±0.005		1.0 ±0.2		2+
2.940			(6)		v. weak		J = 0			0+
2.900			1		v. weak		J = 1			1+
2.773	not 0,4		2,3		2+					2+
2.458	4+	4+			4+	0.084±0.010	0.11±0.04	2.6 ±0.6	2.2±0.7	4+
1.456					2+	0.206±0.010	0.20±0.01	14.4 ±0.15	14.3±1.9	2+

Figure Captions

Fig. 1. $^{58}Ni(p,p')$ energy spectrum at scattering angle 140°.

Fig. 2. $^{60}Ni(p,p')$ energy spectrum at scattering angle 140°.

Fig. 3. $^{120}Sn(p,p')$ energy spectrum at scattering angle 140°.

Fig. 4. $^{58}Ni(\alpha,\alpha')$ energy spectrum at scattering angle 26°.

Fig. 5. Results of the optical model calculations for proton scattering off ^{58}Ni at 17.7 MeV. The cross-section data are presented as ratios to the Rutherford scattering cross sections. The solid line gives the predictions obtained after fitting both cross-section and polarization data, the dotted line is for a fit to the cross-section data alone.

Fig. 6. Results of the optical model calculations for proton scattering off ^{60}Ni at 17.9 MeV. See caption to fig. 5.

Fig. 7. Results of the optical model calculations for proton scattering off ^{120}Sn at 17.8 MeV. See caption to fig. 5.

Fig. 8. Proton inelastic scattering angular distributions for ^{58}Ni. The data for the quadrupole levels is shown in fig. 8(a), for the hexadecapole ($L = 4$) levels in fig. 8(b), and the remaining levels in fig. 8(c). The solid lines give the results of assuming a complex interaction in the DWBA calculations, the dotted lines give the results for a real interaction.

Fig. 9. Proton inelastic scattering angular distributions for ^{60}Ni. The solid lines give the result of assuming a complex interaction in the DWBA calculation, the dotted lines give the results for a real interaction.

Fig. 10. Proton inelastic scattering angular distributions for ^{120}Sn. The data for levels of known spin are given in fig. 10(a), the remainder in fig. 10(b). The solid lines give the results of assuming a complex interaction in the DWBA calculations, the dotted lines give the results for a real interaction.

Fig. 11(a). The elastic scattering angular distribution for 50 MeV α particles from ^{58}Ni is shown, the data being presented as a ratio to the Rutherford scattering cross section. Also presented are the inelastic angular distributions for these levels which are best described as being in phase with the elastic scattering. The 4.106-MeV angular distribution is included also. For the elastic scattering, the curve represents the optical model prediction (see text). For the inelastic levels the appropriate DWBA curves are shown.

Fig. 11(b). The ^{58}Ni(α,α') angular distributions for the levels assigned $J\pi = 2+$. The solid lines are the DWBA L = 2 curves.

Fig. 11(c). The ^{58}Ni(α,α') angular distributions for the levels assigned $J\pi = 4+$. The solid lines are the DWBA L = 4 curves.

$^{58}Ni(p,p')^{58}Ni$ Proton Energy 17.69±0.03 MeV (lab)

Center of mass cross-sections in mb/sr

c.m.	Q = 0 Elastic	Q = -1.456 (2+)	Q = -2.458 (4+)	Q = -2.773 (2+)	Q = -2.900 (1+)
10.2	54,400				
15.3	7,280	4.06 ±0.60	1.72 ±0.34		
20.3	2,086	6.20	1.67		
25.4	851	6.99	1.42	0.234	0.190±0.080
30.5	428	9.55	1.24	0.201	0.325±0.050
35.6	235	10.10	1.16	0.202	0.137±0.020
40.6	163	9.58	1.05	0.170	0.090±0.020
45.7	124	7.75	0.91	0.140	0.100±0.040
50.8	90.6	5.64	0.79	0.100	0.080±0.060
55.8	58.5	3.84	0.88	0.130	0.064±0.030
60.9	29.0	2.72	0.80	0.096	0.050±0.010
65.9	9.60	2.11	0.65	0.086	0.034±0.008
71.0	3.60	--	0.55	0.091	0.040±0.020
76.0	6.05	1.95	0.410	0.104	0.059±0.015
81.0	11.65	2.03	0.315	0.101	0.040±0.008
86.0	15.56	--	0.251	0.098	0.062±0.010
91.0	16.36	1.74	0.255	0.097	0.054±0.008
96.0	13.75	1.47	0.221	0.082	0.072±0.010
101.0	9.65	1.19	0.183	0.089	0.031±0.004
106.0	5.90	1.03	0.171		0.041±0.008
110.9	3.40	0.84	0.186	0.107	--
115.9	2.37	0.72	0.193	0.120	0.025±0.015
120.9	2.19	0.62		0.135	0.034±0.008
125.8	2.75	0.61		0.164	0.036±0.020
130.8	3.58	0.60		0.144	0.060±0.008
135.7	4.12	0.77		0.137	0.060±0.015
140.6	4.89	1.00	0.154	0.112	0.062±0.015
145.6	5.46	1.23	0.152	0.095	0.082±0.030
150.5	5.79	1.46	0.159	0.101	0.082±0.030
155.4	5.70	1.52	0.136		0.110±0.020
160.3	4.95	1.27	0.099		0.100±0.20
165.3	4.95	1.27	0.099		--
170.2	4.44	0.097	0.074	0.154	--
Relative errors	±3%	±4%	±6%	±8%	

Overall normalization error ±5%

(continued)

$^{58}Ni(p,p')^{58}Ni$ Proton Energy 17.69±0.03 MeV (lab)

Center of mass cross-sections in mb/sr

c.m.	Q = -2.940 (0+)	Q = -3.035 (2+)	Q = -3.260 (2+)	Q = -3.414 (3+)	Q = 3.615 (4+)
10.2					
15.3					
20.3					
25.4	0.040±0.040				0.540
30.5	0.120±0.050	0.360	0.481	0.155±0.020	0.458
35.6	0.040±0.020	0.401	0.520		0.498
40.6	0.040±0.030	0.410	0.576	0.131±0.030	0.486
45.7	0.030±0.020	0.327	0.511		0.478
50.8	0.080±0.060	0.288	0.412	0.129	0.475
55.8	0.036±0.025	0.229	0.381	0.093	0.393
60.9	0.060±0.050	0.232	0.283	0.085	0.368
65.9	0.057±0.010	0.186	0.265	0.087	0.308
71.0	0.040±0.020	0.208	0.240	0.093	0.302
76.0	0.029±0.010	0.222	0.245	0.075	0.278
81.0	0.020±0.010	0.245	0.240	0.088	0.256
86.0	0.015±0.010	0.268	0.240	0.082	0.222
91.0	$0.005^{+0.010}_{-0.005}$	0.262	0.221	0.082	0.176
96.0	0.005±0.005	0.266	0.223	0.077	0.175
101.0	0.015±0.010	0.265	0.248	0.085	0.159
106.0	0.021±0.008	0.231	0.231	0.060	0.125
110.9	--	0.246	0.256	0.067	0.120
115.9	0.025±0.015		0.255	0.077	0.103
120.9	0.036±0.009	0.196	0.290	0.080	0.115
125.8	0.036±0.020	0.170		0.090	0.111
130.8	0.031±0.008	0.151	0.196		0.125
135.7	0.060±0.015	0.133	0.202	0.080	0.136
140.6	0.040±0.015	0.117	0.175	0.082	
145.6	0.030±0.030	0.114	0.194	0.079	0.199
150.5	0.020±0.020	0.120	0.214	0.067	0.185
155.4	0.030±0.030	0.147	0.234	0.052	0.181
160.3	<0.030±0.20	0.178	0.262	0.052	0.212
165.3	--	0.192	0.269	0.044	
170.2	--	0.221	0.290		0.199
Relative errors		±7%	±7%	±10%	±7%

Overall normalization error ±5%

(continued)

$^{58}Ni(p,p')^{58}Ni$ Proton Energy 17.69±0.03 MeV (lab)

Center of mass cross-sections in mb/sr

c.m.	Q = -3.773 (3+)	Q = -3.895 (2+)	Q = -4.103 (2)	Q = -4.405 (4+)	Q = -4.472 (3-)
10.2					
15.3					
20.3					
25.4				0.417	0.835
30.5	0.129±0.040	0.319±0.027	0.154		1.18
35.6	0.074±0.020	0.330	0.000	0.405	1.11
40.6	0.117±0.030	0.355	0.103	0.425	1.44
45.7	0.114±0.030	0.294	0.116	0.387	1.65
50.8	0.073±0.025	0.300	0.114	0.465	1.85
55.8	0.060	0.219	0.135	0.406	1.69
60.9	0.042	0.139	0.137	0.406	1.54
65.9	0.051	0.083	0.126	0.382	1.27
71.0	0.056	0.086	0.129	0.411	1.09
76.0	0.049	0.077	0.090	0.356	0.890
81.0	0.055	0.056	0.110	0.375	0.836
86.0	0.065	0.075	0.088	0.327	0.750
91.0	0.062	0.075	0.088	0.299	0.717
96.0	0.065	0.060	0.092	0.278	0.710
101.0	0.067	0.070	0.085	0.245	0.640
106.0	0.066	0.054	0.103	0.231	0.675
110.9	0.049	0.060	0.100	0.208	0.658
115.9	0.055	0.049	0.096	0.199	0.666
120.9	0.046	0.046	0.090	0.167	0.675
125.8	0.057	0.044	0.087	0.180	0.617
130.8	0.046	0.041	0.091	0.196	0.606
135.7	0.051	0.042	0.079	0.168	0.539
140.6	0.049	0.044	0.090	0.141	0.498
145.6		0.045	0.071	0.127	0.440
150.5		0.056	0.064	0.143	0.390
155.4	0.038		0.064	0.147	0.343
160.3	0.032		0.072	0.130	0.272
165.3	0.021		0.072	0.115	0.194
170.2	0.018	0.046	0.071	0.109	0.123
Relative errors	±15%	±15%	±10%	±15%	±7%

Overall normalization error ±5%.

(continued)

$^{58}Ni(p,p')^{58}Ni$ Proton Energy 17.69±0.03 MeV (lab)

Center of mass cross-sections in mb/sr

c.m.	Q = -4.75 (4+)	Q = -5.59 (4+)
10.2		
15.3		
20.3		
25.4	1.12	0.587
30.5		0.655
35.6	0.811	0.435
40.6	0.720	0.525
45.7	0.820	0.561
50.8	0.670	0.570
55.8	0.616	0.346
60.9	0.726	0.460
65.9	0.685	
71.0	0.610	0.496
76.0	0.478	0.472
81.0	0.411	0.418
86.0	0.290	0.350
91.0	0.284	0.350
96.0	0.241	0.326
101.0	0.247	0.265
106.0	0.205	0.252
110.9	0.226	0.250
115.9	0.204	0.245
120.9	0.181	0.244
125.8	0.156	0.216
130.8	0.132	0.212
135.7	0.149	0.175
140.6	0.144	0.194
145.6	0.149	0.186
150.5	0.151	0.188
155.4	0.178	0.175
160.3	0.176	0.172
165.3	0.193	0.165
170.2	0.173	0.162
Relative errors	±7%	±10%

Overall normalization error ±5%

$^{60}Ni(p,p')^{60}Ni$ Proton Energy 17.91±0.05 MeV (lab)

Center of mass cross-sections in mb/sr

c.m.	Q=0 elastic	Q=-1.332 2+	Q=-2.159 2+	Q=-2.286 0+	Q=-2.505 4+	Q=-3.119 2+	Q=-4.038 3-
15.2	5754.	2.96	---	---	---	---	---
20.3	1663.	4.73	---	---	1.54	---	---
25.4	746.	6.77	---	---	1.17	---	---
30.5	372.	9.10	0.074	---	1.00	0.354	0.94
35.6	192.	9.46	0.068	---	0.71	0.270	1.19
40.6	131.	8.92	0.082	---	0.77	0.244	1.57
45.7	94.0	6.76	0.078	---	0.73	0.197	1.77
50.7	68.9	5.03	0.058	0.022	0.68	0.221	1.85
55.8	41.2	3.37	0.058	0.033	0.68	0.221	1.75
60.8	18.4	2.25	0.051	0.031	0.58	0.189	1.54
63.4	10.5	2.06	0.055	0.025	0.57	0.212	1.36
65.9	5.75	---	0.057	0.028	0.52	0.200	1.16
68.4	3.45	1.80	0.055	0.034	0.50	0.189	1.07
70.9	3.00	1.69	0.032	0.029	0.407	0.175	0.935
73.4	4.61	1.79	0.026	0.040	0.383	0.170	0.930
75.9	6.56	1.73	0.027	0.032	0.312	0.163	0.774
78.5	9.51	1.84	0.036	0.049	0.298	0.166	0.732
81.0	11.1	---	0.028	0.015	0.218	0.133	0.646
86.0	14.0	1.66	0.034	0.010	0.166	0.095	0.641
91.0	13.1	1.47	---	---	0.135	0.084	0.595
96.0	10.6	1.32	0.028	0.007	0.131	0.066	0.642
101.0	6.35	1.12	0.023	0.005	0.104	0.050	0.539
105.9	3.68	0.98	0.015	0.016	0.100	0.049	0.628
110.9	1.84	0.83	0.017	0.018	0.085	0.045	0.580
115.9	1.62	0.78	---	0.023	0.086	---	0.566
120.8	2.03	0.66	0.015	---	0.082	0.046	0.535
125.8	2.71	0.59	0.026	0.022	0.090	0.049	0.513
130.7	3.18	0.56	0.031	0.014	---	0.043	0.496
135.7	3.42	0.62	0.034	0.011	0.076	0.058	0.458
140.6	3.56	0.78	0.046	0.006	0.076	0.068	0.434
145.6	3.66	0.94	0.053	0.006	0.088	0.067	0.376
150.5	3.49	1.13	0.067	0.009	0.083	0.064	0.308
155.4	3.44	1.16	0.070	0.007	0.079	0.058	0.284
160.3	3.08	1.10	0.056	0.009	0.080	0.068	---
165.3	2.64	0.92	0.059	0.004	0.054	0.060	---
Relative errors	±3%	±4%	±15%	±25%	±10%	±15%	±6%

Overall normalization error ±5%

$^{120}Sn(p,p')^{120}Sn$ Proton energy 17.70±0.05 MeV

Center of mass cross-sections in mb/sr

c.m.	Q = 0 (0+)	Q = -1.166 (2+)	Q = -2.183 (4+)	Q = -2.272 (5-)	Q = -2.391 (3-)
20.2	10600				
25.2	4390				
30.2	1953				
35.3	726				
40.3	270				
45.1	148	1.24	0.191	0.423	1.85
50.2	127.5	1.13	0.176	0.444	1.43
55.2	116	1.45	0.157	0.461	0.975
60.2	95.0	1.56	0.118	0.443	0.707
65.2	69.3	1.60	0.085	0.400	0.705
70.2	41.4	1.33	0.073	0.339	0.918
75.3	20.6	0.936	0.074	0.223	1.019
80.3	10.0	0.594	0.085	0.167	1.08
85.3	7.43	0.397	0.081	---	1.062
90.3	8.95	0.295	0.065	0.168	0.818
95.3	11.4	0.351	0.060	0.163	0.612
100.3	11.9	0.430	---	0.152	0.412
105.3	10.4	---	0.052	---	0.287
110.2	7.92	0.450	0.054	0.168	---
115.2	5.02	0.391	0.045	0.154	0.265
120.2	2.83	---	---	---	---
125.2	1.90	0.194	0.039	0.114	0.341
130.2	1.98	0.155	0.036	0.104	0.373
135.1	2.45	0.153	0.028	0.081	0.356
140.1	2.86	0.161	0.027	0.070	0.322
145.1	2.92	0.187	0.028	0.060	0.274
150.0	2.57	0.229	0.021	0.052	0.239
155.0	2.31	0.280	0.023	0.040	0.209
160.0	1.79	0.320	0.020	0.042	0.172
164.9	1.27	0.343	0.025	0.045	0.121
169.9	0.700	0.304	0.021	0.039	0.090
Relative errors	±3%	±6%	±10%	±8%	±6%

(continued)

$^{120}Sn(p,p')^{120}Sn$ Proton energy 17.70±0.05 MeV

Center of mass cross-sections in mb/sr

c.m.	Q = -2.455 (4+)	Q = -2.67 (4+)	Q = -3.06 (4+)	Q = -3.17 (4+)	Q = -3.45 (3-)
20.2					
25.2					
30.2					
35.3					
40.3					
45.1	0.403		0.182	0.388	0.127
50.2	0.333		0.166	0.310	0.093
55.2	0.316		0.132	0.287	0.094
60.2	0.263	0.064	0.104	0.236	0.088
65.2	0.211	0.059	0.065	0.179	0.076
70.2	0.165	0.063	0.042	0.139	0.078
75.3	0.165	0.051	0.035	0.095	0.090
80.3	0.155	0.043	0.032	0.086	0.091
85.3	0.158	0.045	0.042	0.094	0.081
90.3	---	0.082	0.050	0.098	0.074
95.3	0.179	---	0.047	0.106	0.056
100.3	0.160	0.044	0.048	0.106	0.041
105.3	0.130	0.039	---	0.124	0.040
110.2	0.126	0.035	0.032	0.083	0.041
115.2	0.100	0.028	0.038	---	---
120.2	---	---	---	---	---
125.2	0.068	---	0.016	0.057	0.044
130.2	0.057	0.018	0.014	0.046	0.038
135.1	0.057	0.016	---	0.046	0.037
140.1	0.050	0.012	0.019	0.057	0.030
145.1	0.056	0.017	0.020	---	0.028
150.0	0.057	0.016	0.020	0.049	---
155.0	0.066	0.018	0.019	0.046	0.044
160.0	0.064	0.020	0.026	0.049	
164.9	0.078	0.019	0.022	0.050	
169.9	0.072	0.024	0.020	0.044	
Relative errors	±8%	±8%	±10%	±8%	±8%

$^{58}Ni(\alpha,\alpha')^{58}Ni$ E_α = 50.2 MeV (lab)

Center of mass cross-sections in mb/sr

c.m.	Q = 0 Elastic	Q = -1.456 (2+)	Q = -2.458 (4+)	Q = -2.773 (2+)	Q = -3.035 (2+)
10.7	11795±446	57.9	3.0 ±1.0		2.2 ±0.7
12.8	4347±444	24.9	3.73	0.50 ±0.30	2.68 ±0.37
15.0	2429	2.8 ±0.8	3.80	0.17 ±0.05	0.53
17.1	1390±30	13.7	3.16	0.349	0.89
19.2	341	26.9	1.03	0.122	1.43
21.4	138	13.2	0.22	0.142	0.06
23.5	235	1.54	0.74	0.150	0.34
25.6	184	3.10	1.42	0.090	0.066
26.7	110				
27.7	50.2	9.78	1.00		0.49
28.8	12.3	10.1	0.61		0.84
29.9	5.07	8.32	0.37	0.138	
30.9	16.5	5.39	0.186	0.207	0.58
32.0	30.8	2.40		0.184	0.44
33.0	39.4	0.709		0.201	0.27
34.1	40.7	0.523	0.38		0.093
35.1	31.8	1.64	0.48		0.049±0.010
36.2	19.5	3.06	0.46	0.074	
37.3	7.58	4.21	0.33	0.032	0.192
38.3	1.31	4.33	0.235	0.020	0.237
39.4	3.90	3.88	0.143	0.025	0.210
40.4	3.64	2.64	0.078	0.053	0.212
41.5	7.54	1.57	0.091	0.079	0.173±0.016
42.6	10.7	0.81	0.155	0.074	0.113
43.6	11.1	0.57	0.162	0.072	0.061±0.010
44.7	9.50	0.80	0.239	0.071	0.038±0.004
45.7	6.70	1.26	0.224	0.060	0.031±0.006
46.8	3.58	1.65	0.201	0.034	0.045±0.006
47.8	1.66	1.90	0.171	0.017±0.005	0.063±0.009
49.9	0.951	1.44	0.105	0.014±0.005	0.085±0.011
51.0	1.88	1.08	0.094	0.016	0.066±0.006
53.0	3.52	0.535	0.118	0.025	0.028±0.004
55.1	2.83	0.540	0.129		0.025±0.003
57.2	1.33	0.804	0.115	0.011±0.002	0.028±0.003
59.3	0.458	0.827	0.078	0.006±0.002	
61.4	0.546	0.573	0.058	0.008±0.002	0.031±0.003
63.4	0.821	0.300	0.050	0.012±0.002	0.017±0.002
Relative errors (unless specified)	±5%	±5%	±6%	±10%	±6%

$^{58}Ni(\alpha,\alpha')^{58}Ni$ E_α = 50.2 MeV (lab)

Center of mass cross-sections in mb/sr

c.m.	Q = -3.260 (2+)	Q = -3.524 (4+)	Q = -3.615 (4+)	Q = -3.895 (2+)	Q = -4.103 (2+)
10.7	3.9 ±0.5	0.40 ±0.40	1.00 ±0.40		
12.8	3.9 ±0.5	0.50 ±0.20	1.20 ±0.40	1.18 ±0.30	
15.0	0.74 ±0.10	0.20 ±0.10	1.60	0.225	0.23 ±0.08
17.1	0.94	0.37	1.52	0.40	0.431±0.025
19.2	1.69	0.38	0.63	0.56	0.197
21.4	1.41	0.144	0.139	0.34	0.155
23.5	0.46	0.072	0.195	0.067	0.099
25.6	0.136	0.162	0.44	0.101	0.066
26.7				0.225	
27.7	0.58	0.219	0.42	0.245	0.080
28.8	0.89	0.180	0.33	0.232	0.063±0.010
29.9	0.95	0.142	0.240	0.164	
30.9			0.136	0.103±0.13	0.076±0.010
32.0	0.61			0.038±0.010	0.066
33.0	0.36				0.055±0.008
34.1	0.213	0.121	0.080±0.008		
35.1		0.135±0.014	0.143±0.014	0.039±0.006	
36.2	0.107	0.118	0.157	0.083±0.010	0.053
37.3	0.326	0.094±0.011	0.156	0.087±0.010	0.050±0.008
38.3	0.283	0.093±0.010	0.147	0.083	0.046±0.006
39.4	0.308			0.052±0.010	0.044±0.008
40.4	0.281	0.033±0.003			0.044±0.008
41.5		0.017±0.005	0.035±0.006		
42.6	0.168	0.025±0.003	0.038±0.003	0.018±0.002	
43.6	0.113±0.012	0.030±0.010	0.042±0.008	0.027±0.006	0.056±0.009
44.7	0.049±0.005	0.030±0.005	0.077	0.025±0.003	0.044
45.7	0.031±0.006	0.055±0.010	0.071±0.009	0.042±0.010	0.044±0.008
46.8		0.041±0.004	0.072	0.041	0.034
47.8	0.053±0.009	0.023±0.006	0.050±0.008	0.063±0.010	0.023±0.006
49.9	0.085±0.011	0.028±0.006	0.025±0.006	0.035±0.006	0.027±0.006
51.0	0.100	0.019	0.030±0.003	0.021±0.002	0.055
53.0	0.058	0.013	0.014±0.002	0.015±0.002	0.033
55.1	0.025±0.003	0.031	0.027±0.003	0.017±0.002	0.028
57.2	0.031±0.003	0.033±0.003	0.030±0.003	0.018±0.002	0.020±0.003
59.3	0.055±0.005	0.025±0.003	0.028±0.003	0.016±0.002	0.019
61.4		0.020±0.003	0.020±0.003	0.014±0.002	0.019
63.4	0.045±0.003	0.031±0.003	0.008±0.001		0.020±0.003
Relative errors (unless specified)	±6%	±6%	±6%	±7%	±10%

$^{58}Ni(\alpha,\alpha')^{58}Ni$ E_α = 50.2 MeV (lab)

Center of mass cross-sections in mb/sr

c.m.	Q = -4.405 (4+)	Q = -4.472 (3-)	Q = -4.75 (4+)	Q = -5.59 (4+)
10.7	1.40 ±0.40	19.0 ±1.0		
12.8	1.30 ±0.60	19.3	2.33 ±0.35	2.65 ±0.80
15.0	3.00 ±1.00	12.5	3.12	1.45
17.1	2.90 ±0.30	3.28	2.65	0.83 ±0.40
19.2	1.61	2.04	1.51	0.96
21.4	0.242	5.71	0.45	0.50
23.5		6.51	0.39	0.20 ±0.05
25.6	0.59	3.68	0.86	0.30
26.7				0.39
27.7	0.97	0.87	0.95	0.51
28.8	0.72	0.76	0.84	0.45
29.9	0.64	1.36	0.51	0.40 ±0.20
30.9	0.62	1.78	0.31	0.41
32.0	0.33 ±0.6	2.41	0.20	0.21 ±0.04
33.0		2.48	0.133±0.013	0.164
34.1		2.28	0.215	0.109
35.1		1.62	0.238	0.113±0.011
36.2		1.56	0.38	0.139
37.3	0.40	0.79	0.47	0.230
38.3	0.42	0.31		0.224
39.4	0.31	0.47	0.281	0.250
40.4	0.251	0.70	0.171	0.165±0.37
41.5	0.141±0.014	0.82	0.121±0.014	
42.6				0.078±0.030
43.6		0.99	0.055±0.010	0.124±0.013
44.7				0.066
45.7		0.48		0.096
46.8	0.133	0.32		0.103
47.8	0.133	0.28 ±0.02	0.127±0.013	0.108±0.015
49.9	0.127±0.013	0.28 ±0.02	0.105±0.012	0.139
51.0	0.119	0.38	0.080	
53.0	0.075	0.45	0.039±0.004	0.051±0.015
55.1		0.40	0.036	0.069
57.2	0.055	0.179	0.067	
59.3	0.094	0.129	0.069	0.075
61.4	0.088	0.129	0.039	0.072
63.4	0.044	0.158	0.028±0.003	
Relative errors (unless specified)	±6%	±6%	±6%	±7%

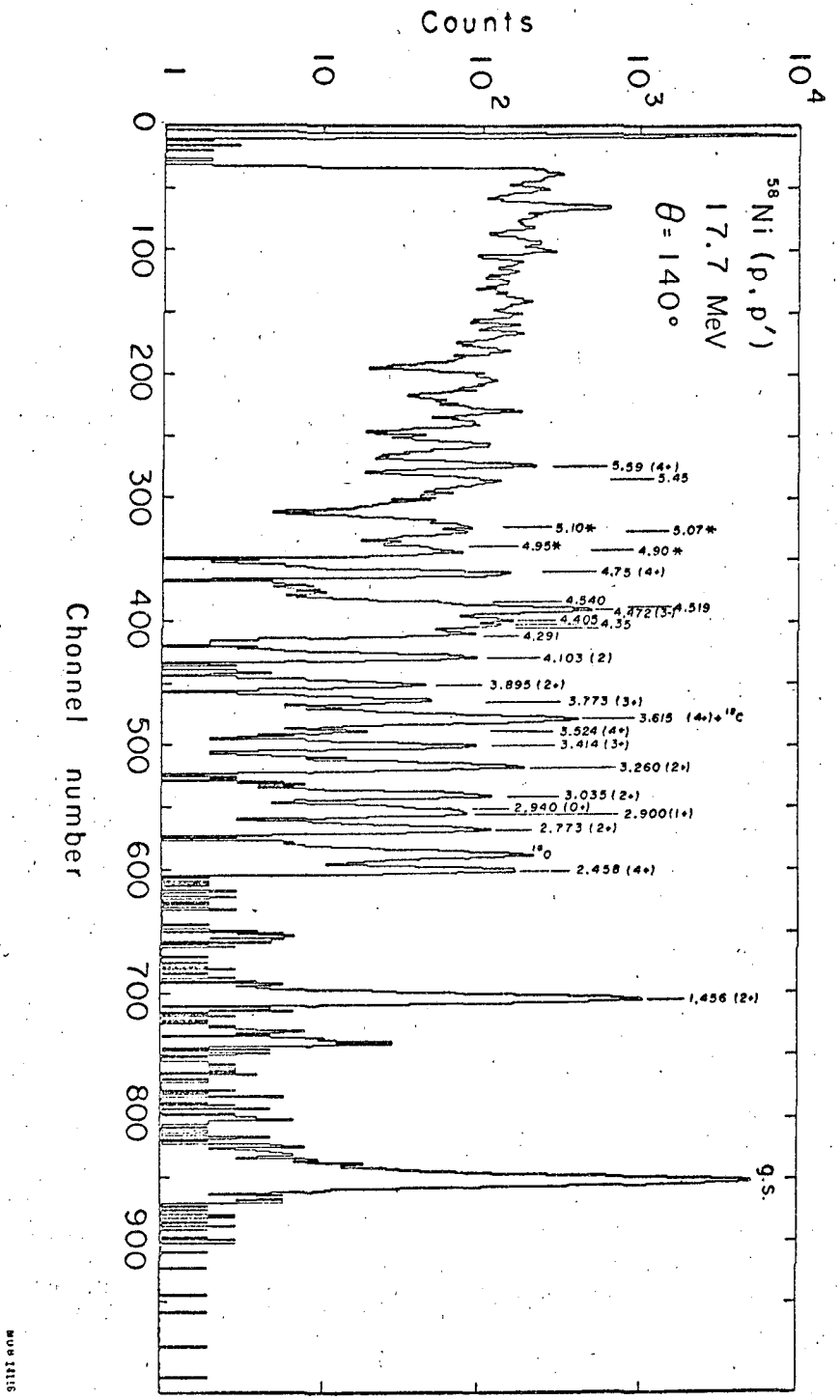
Counts
1
10
10²
10³
10⁴
0
100
200
300
400
500
600
700
800
900
Channel number
⁵⁸Ni (p, p')
17.7 MeV
θ = 140°
5.59 (4+)
5.45
5.10*
5.07*
4.95*
4.90*
4.75 (4+)
4.540
4.472 (3-)
4.519
4.405
4.35
4.291
4.103 (2)
3.895 (2+)
3.773 (3+)
3.615 (4+)+¹²C
3.524 (4+)
3.414 (3+)
3.260 (2+)
3.035 (2+)
2.940 (0+)
2.900 (1+)
2.773 (2+)
¹⁶O
2.458 (4+)
1.456 (2+)
g.s.

Fig. 1.

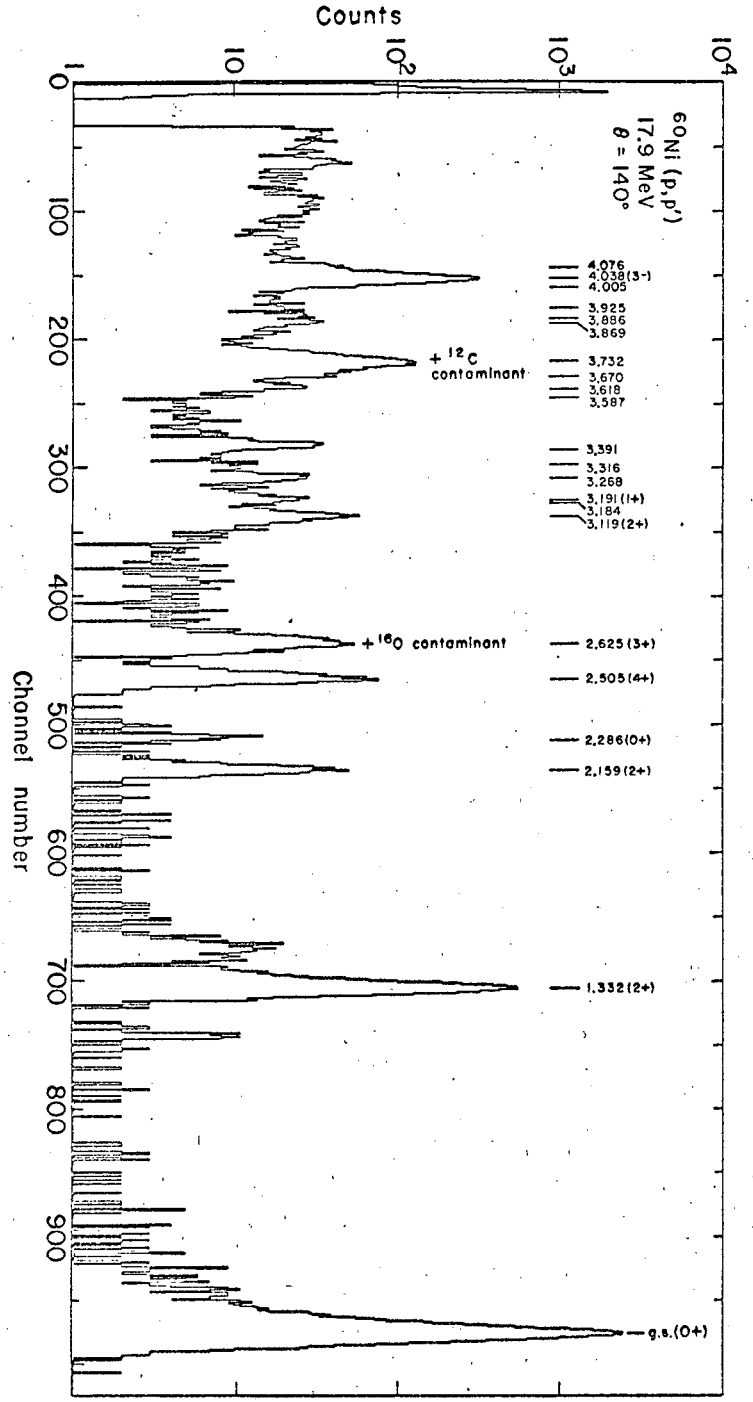
Counts
1
10
10²
10³
10⁴
0
100
200
300
400
500
600
700
800
900
Channel number
⁶⁰Ni (p,p')
17.9 MeV
θ = 140°
4.076
4.038(3-)
4.005
3.925
3.886
3.869
+ ¹²C contaminant
3.732
3.670
3.618
3.587
3.391
3.316
3.268
3.191(1+)
3.184
3.119(2+)
+ ¹⁶O contaminant
2.625(3+)
2.505(4+)
2.286(0+)
2.159(2+)
1.332(2+)
g.s.(0+)

Fig. 2.

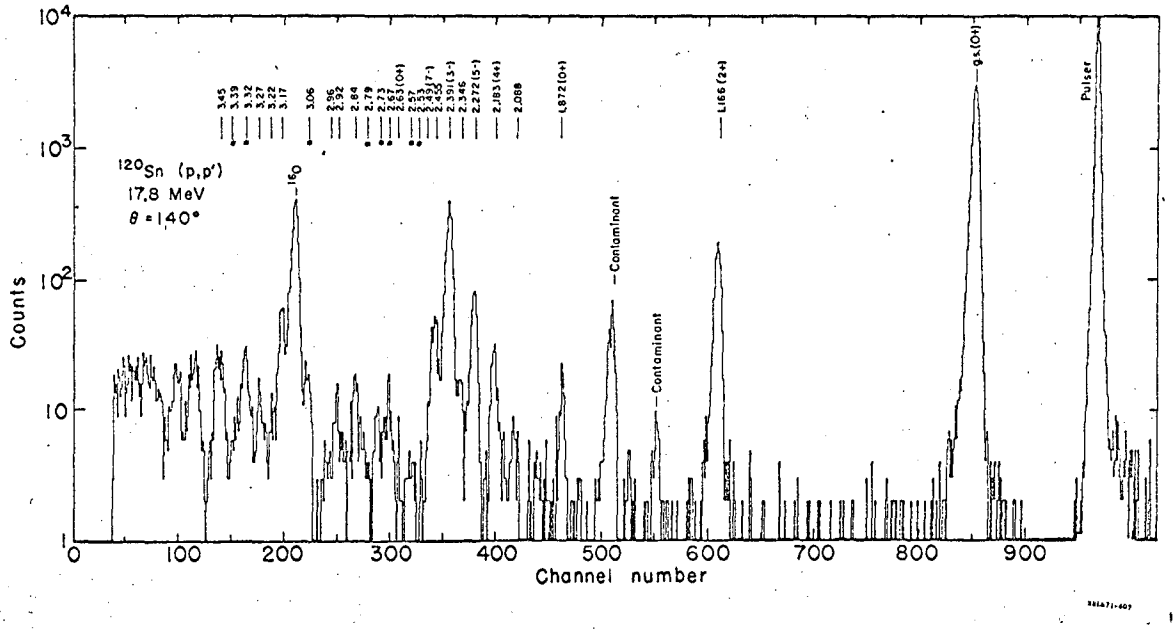
^{120}Sn (p,p')
17.8 MeV
θ = 140°
16O
Contaminant
Contaminant
L166 (2+)
gs (0+)
Pulser
Counts
Channel number

Fig. 3.

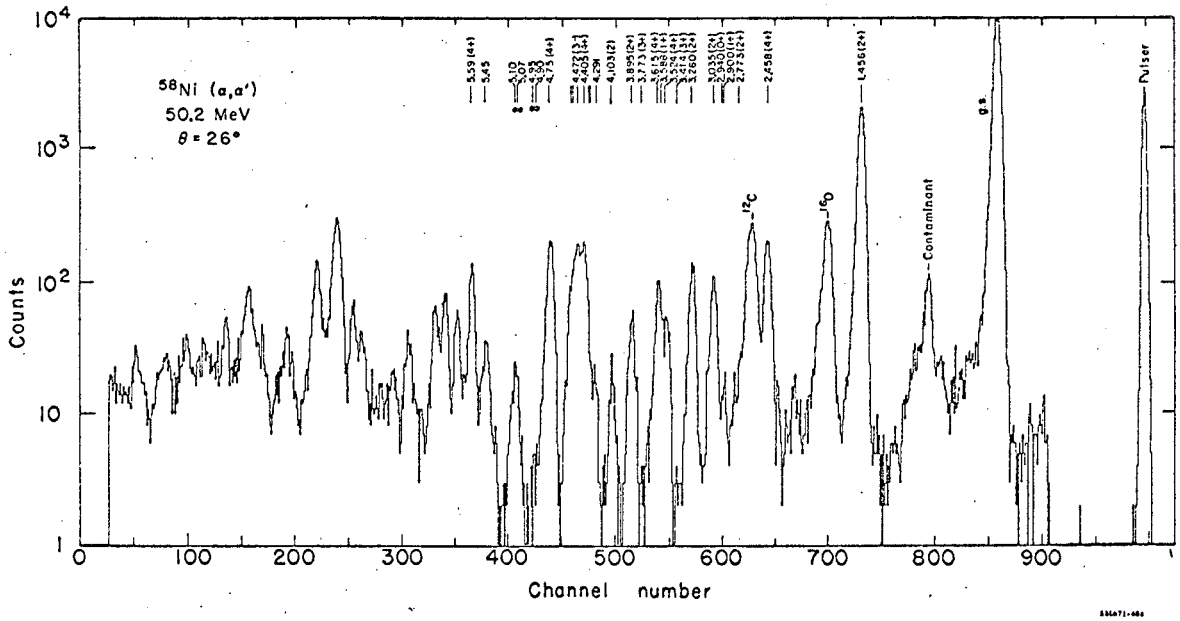
^{58}Ni (a,a')
50.2 MeV
θ = 26°
Counts
Channel number
Pulser
Contaminant
^{12}C
^{16}O
g.s.

Fig. 4.

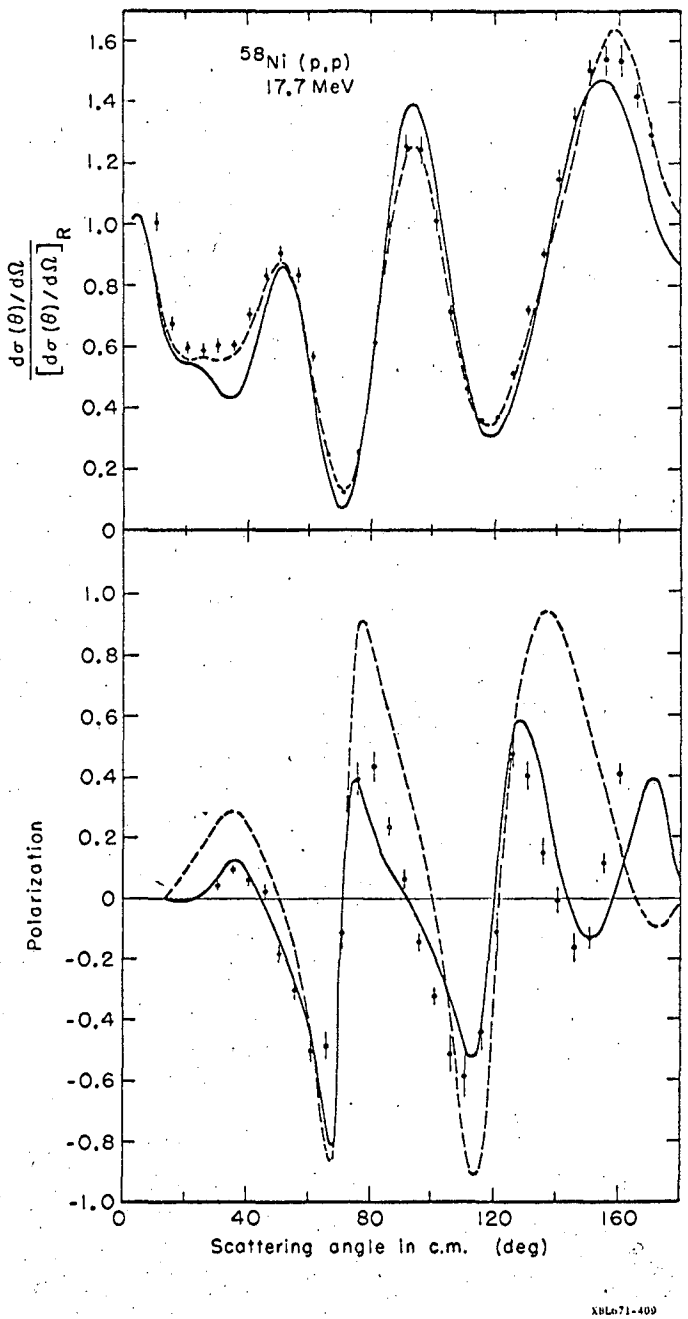
58Ni (p,p)
17.7 MeV
dσ(θ)/dΩ / [dσ(θ)/dΩ]R
Polarization
Scattering angle in c.m. (deg)
XBL071-409

Fig. 5.

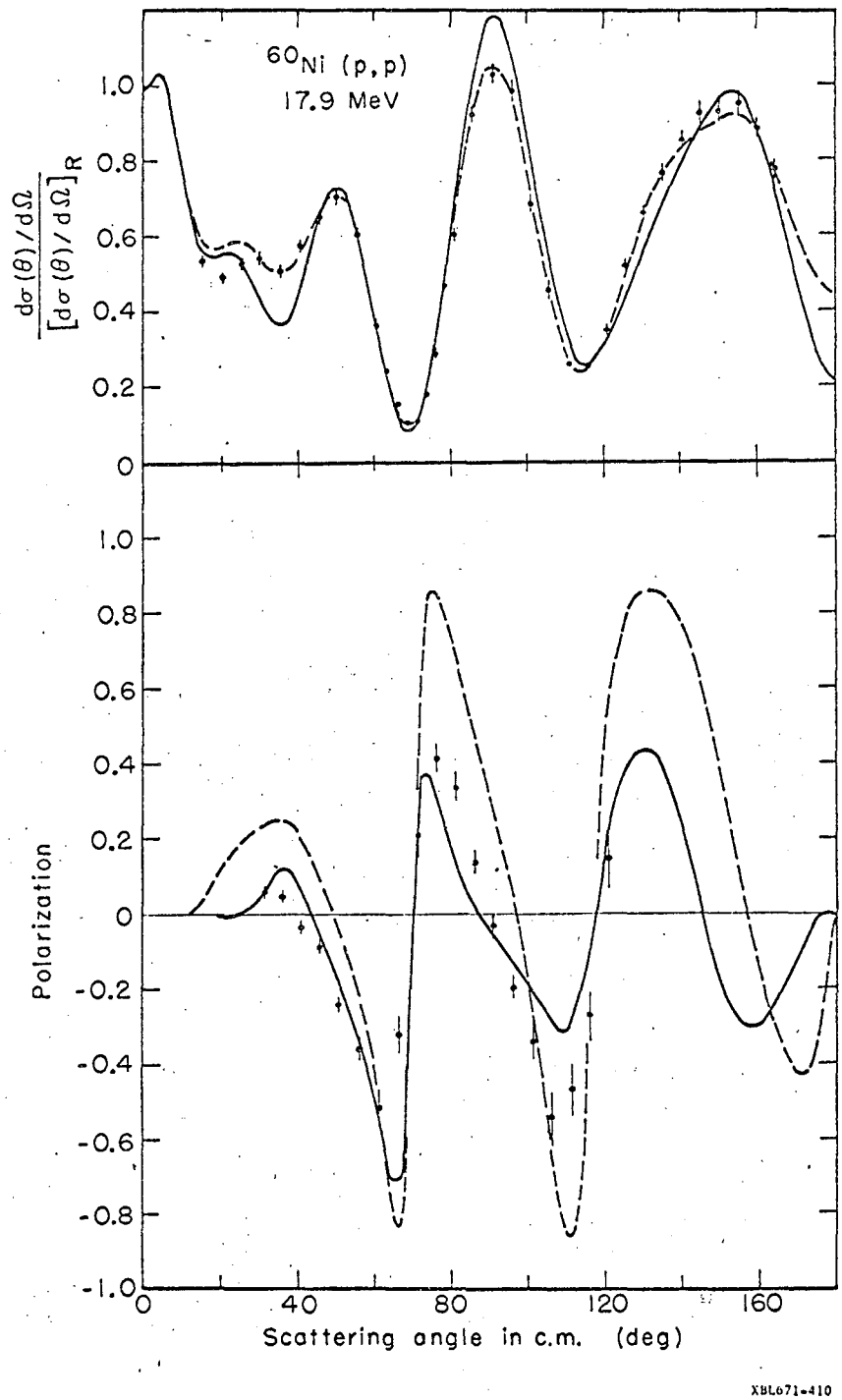
^{60}Ni (p,p)
17.9 MeV
$\frac{d\sigma(\theta)/d\Omega}{[d\sigma(\theta)/d\Omega]_R}$
1.0
0.8
0.6
0.4
0.2
0
Polarization
1.0
0.8
0.6
0.4
0.2
0
-0.2
-0.4
-0.6
-0.8
-1.0
0
40
80
120
160
Scattering angle in c.m. (deg)
XBL671-410

Fig. 6.

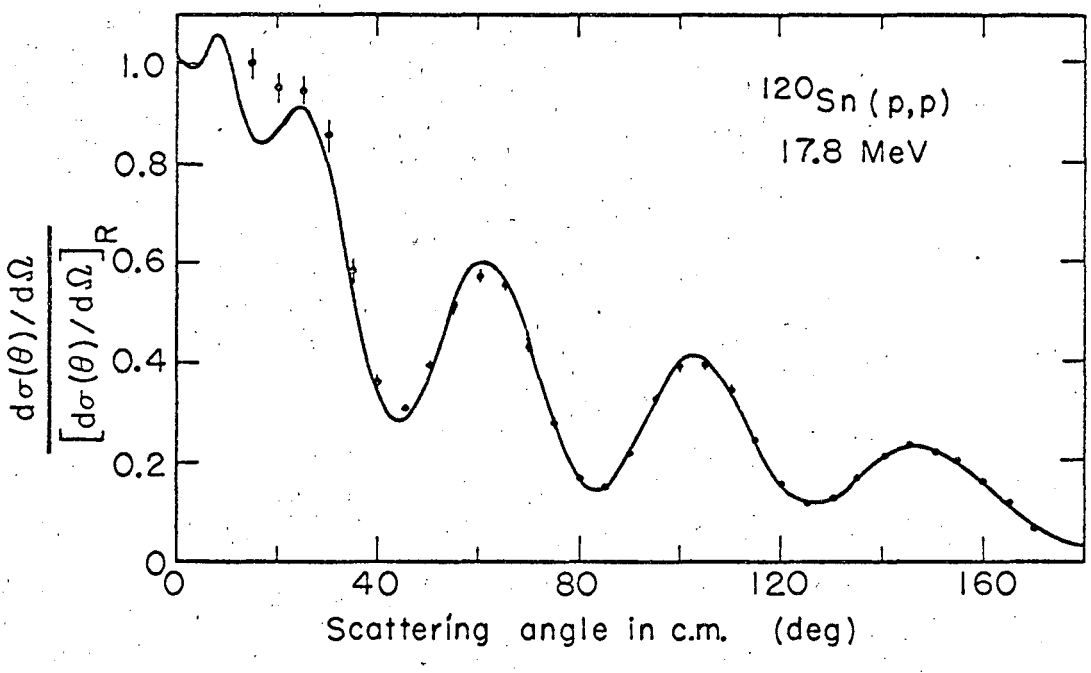

XBL671-411

Fig. 7.

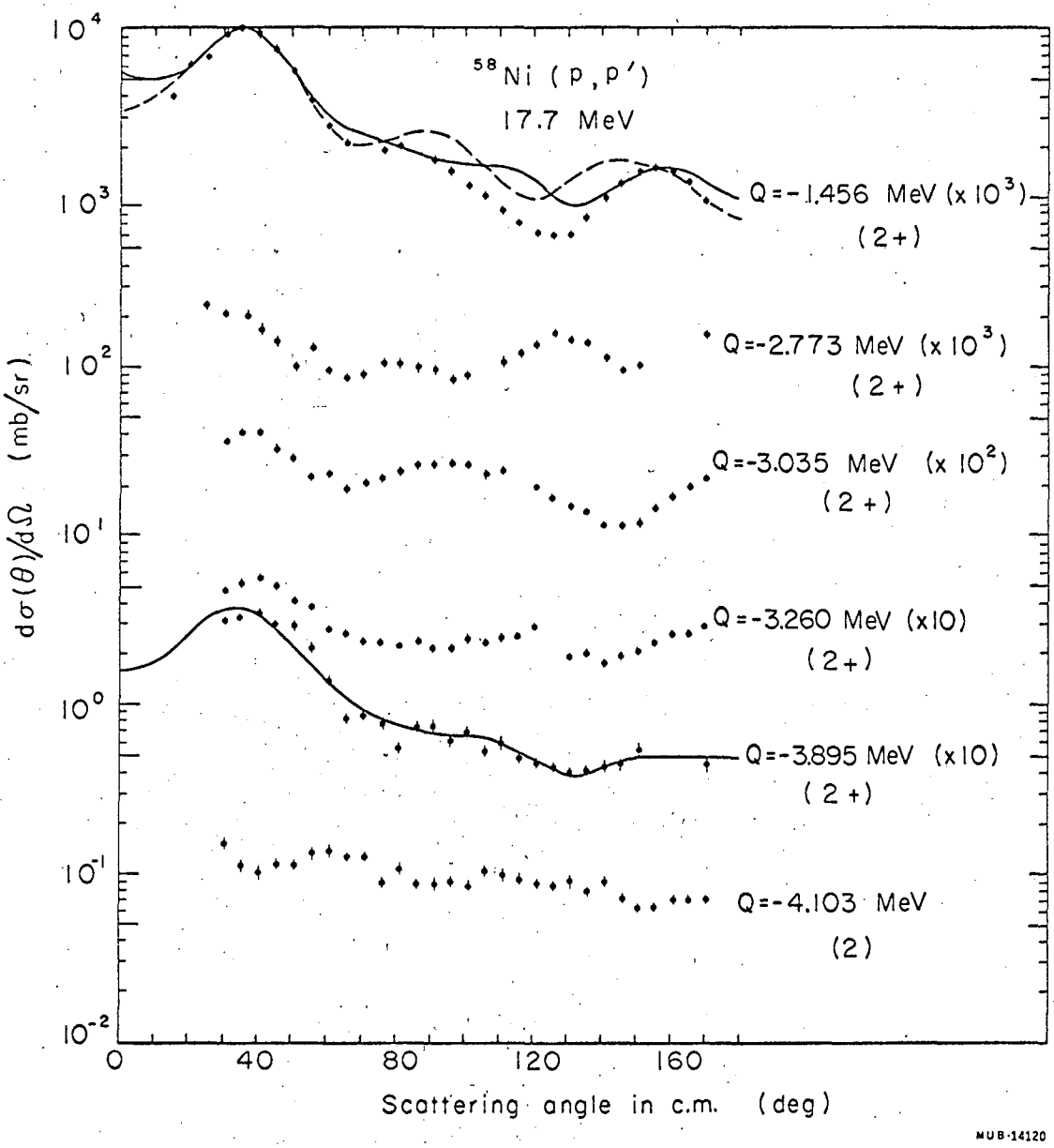
^{58}Ni (p,p')
17.7 MeV
Q=-1.456 MeV (x 10^3)
(2+)
Q=-2.773 MeV (x 10^3)
(2+)
Q=-3.035 MeV (x 10^2)
(2+)
Q=-3.260 MeV (x10)
(2+)
Q=-3.895 MeV (x10)
(2+)
Q=-4.103 MeV
(2)
$d\sigma(\theta)/d\Omega$ (mb/sr)
Scattering angle in c.m. (deg)
MUB-14120

Fig. 8(a).

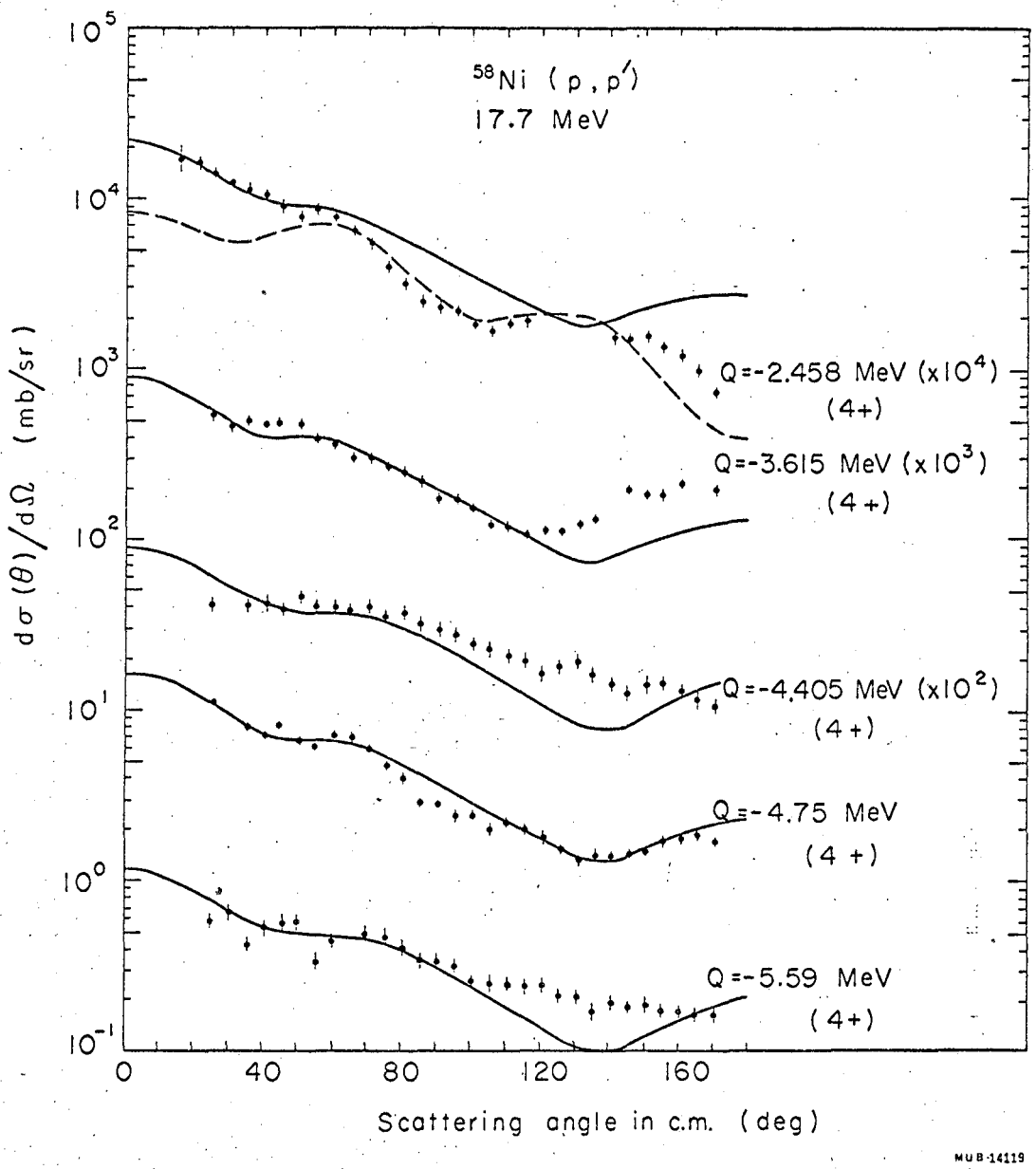
^{58}Ni (p , p′)
17.7 MeV
Q=-2.458 MeV (x10^4)
(4+)
Q=-3.615 MeV (x10^3)
(4+)
Q=-4.405 MeV (x10^2)
(4+)
Q=-4.75 MeV
(4+)
Q=-5.59 MeV
(4+)
dσ(θ)/dΩ (mb/sr)
Scattering angle in c.m. (deg)
MUB-14119

Fig. 8(b).

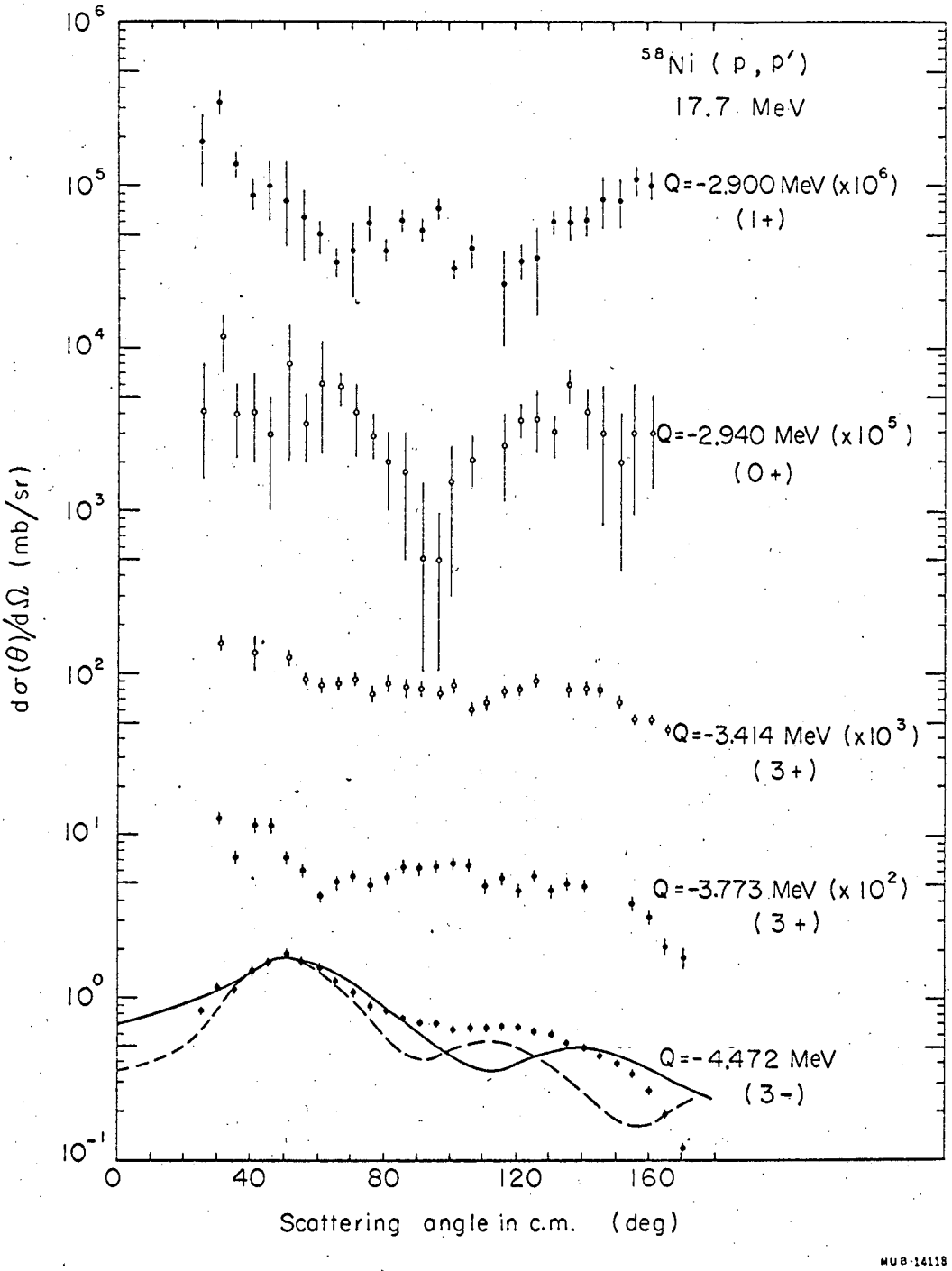
^{58}Ni (p , p′)
17.7 MeV
Q=-2.900 MeV (x10^6)
(1+)
Q=-2.940 MeV (x10^5)
(0+)
Q=-3.414 MeV (x10^3)
(3+)
Q=-3.773 MeV (x 10^2)
(3+)
Q=-4.472 MeV
(3-)
dσ(θ)/dΩ (mb/sr)
Scattering angle in c.m. (deg)
MUB-14118

Fig. 8(c).

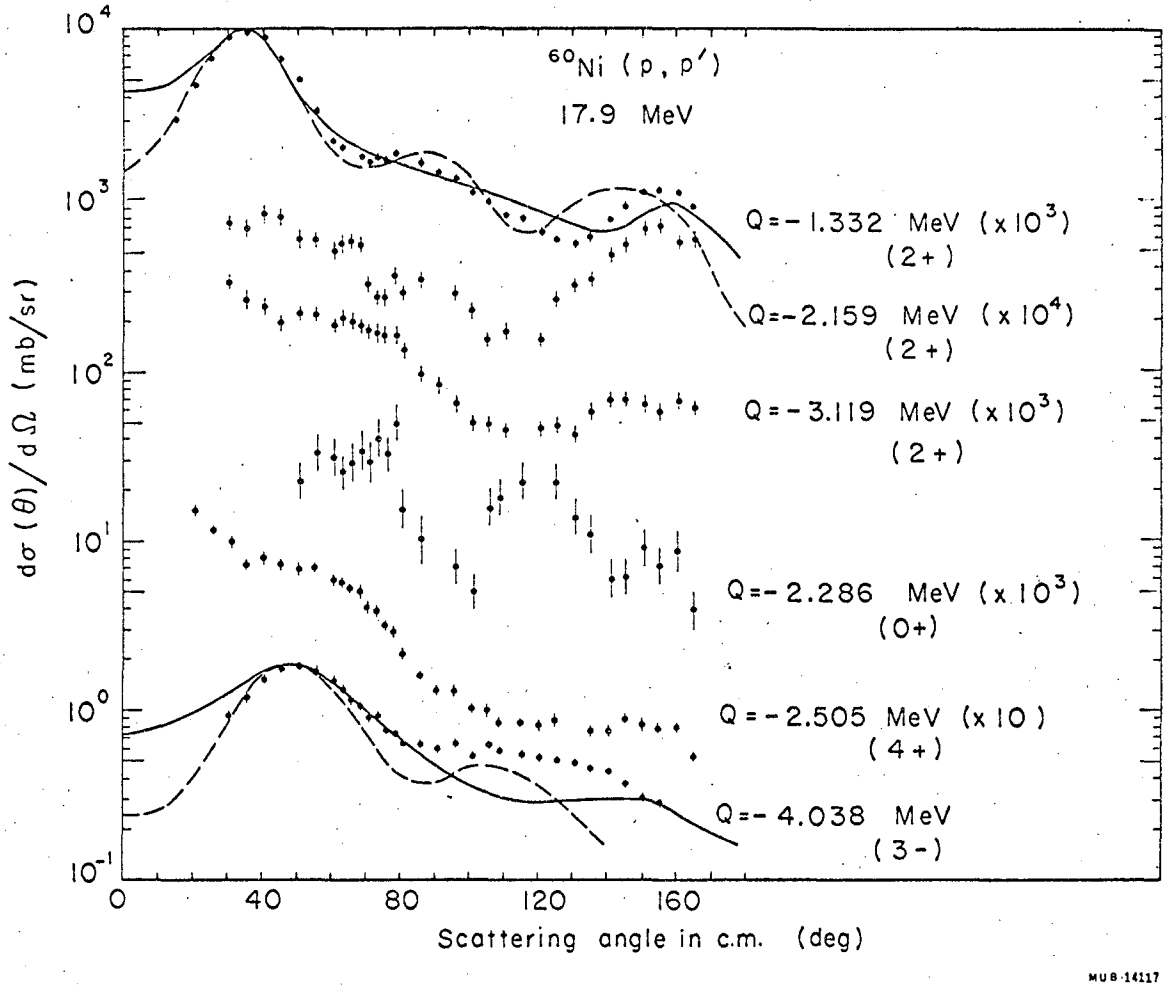
^{60}Ni (p, p′)
17.9 MeV
Q = - 1.332 MeV (x 10^3)
(2+)
Q = - 2.159 MeV (x 10^4)
(2+)
Q = - 3.119 MeV (x 10^3)
(2+)
Q = - 2.286 MeV (x 10^3)
(0+)
Q = - 2.505 MeV (x 10)
(4+)
Q = - 4.038 MeV
(3-)
$d\sigma(\theta)/d\Omega$ (mb/sr)
Scattering angle in c.m. (deg)
MUB-14117

Fig. 9.

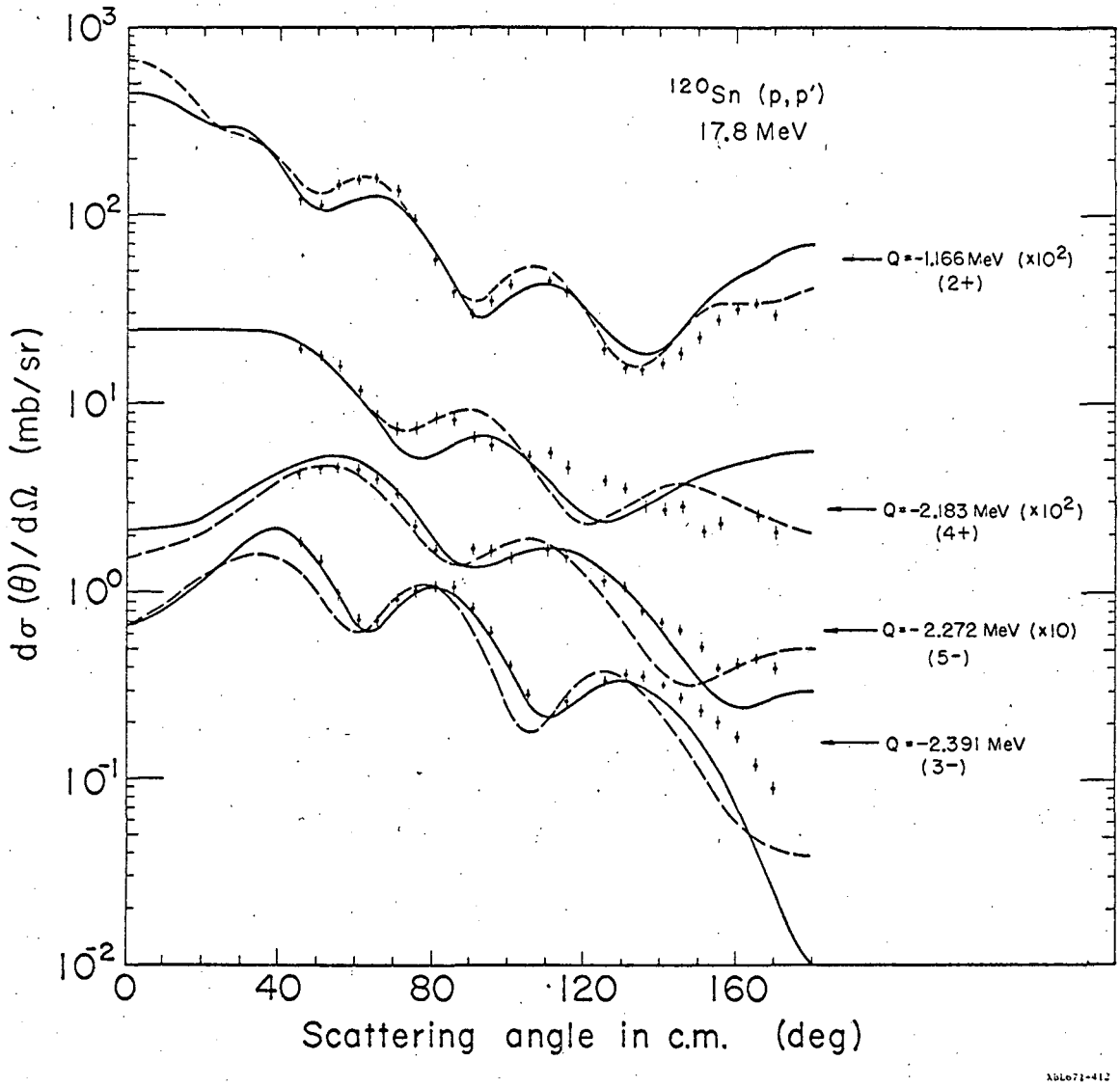
^{120}Sn (p,p')
17.8 MeV
Q=-1.166 MeV (x10^2)
(2+)
Q=-2.183 MeV (x10^2)
(4+)
Q=-2.272 MeV (x10)
(5-)
Q=-2.391 MeV
(3-)
dσ (θ)/dΩ (mb/sr)
Scattering angle in c.m. (deg)
XBL071-412

Fig. 10(a).

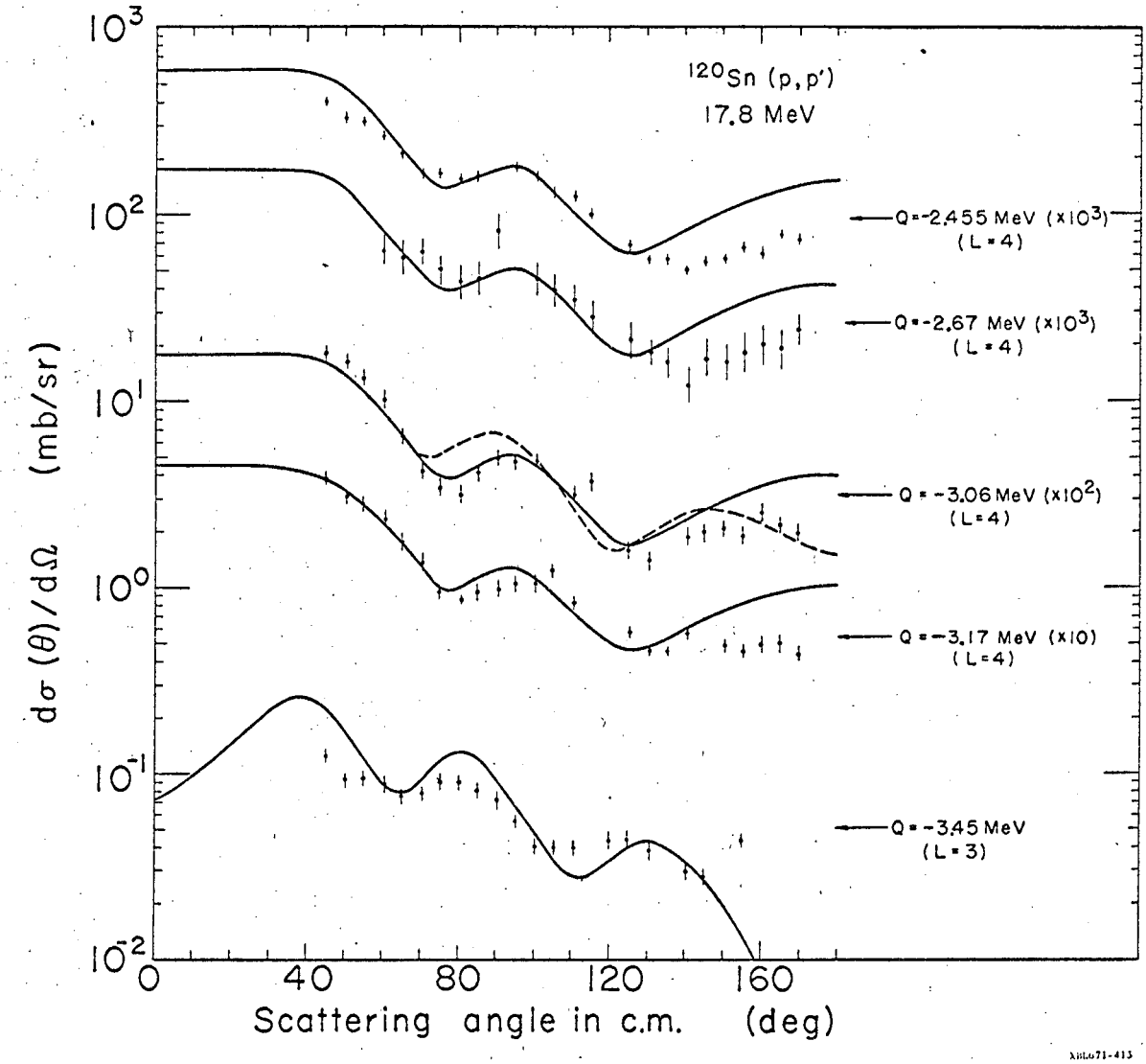
^{120}Sn (p, p')
17.8 MeV
Q = -2.455 MeV (x10^3)
(L = 4)
Q = -2.67 MeV (x10^3)
(L = 4)
Q = -3.06 MeV (x10^2)
(L = 4)
Q = -3.17 MeV (x10)
(L = 4)
Q = -3.45 MeV
(L = 3)
$d\sigma(\theta)/d\Omega$ (mb/sr)
Scattering angle in c.m. (deg)
0
40
80
120
160
10^3
10^2
10^1
10^0
10^{-1}
10^{-2}

Fig. 10(b).

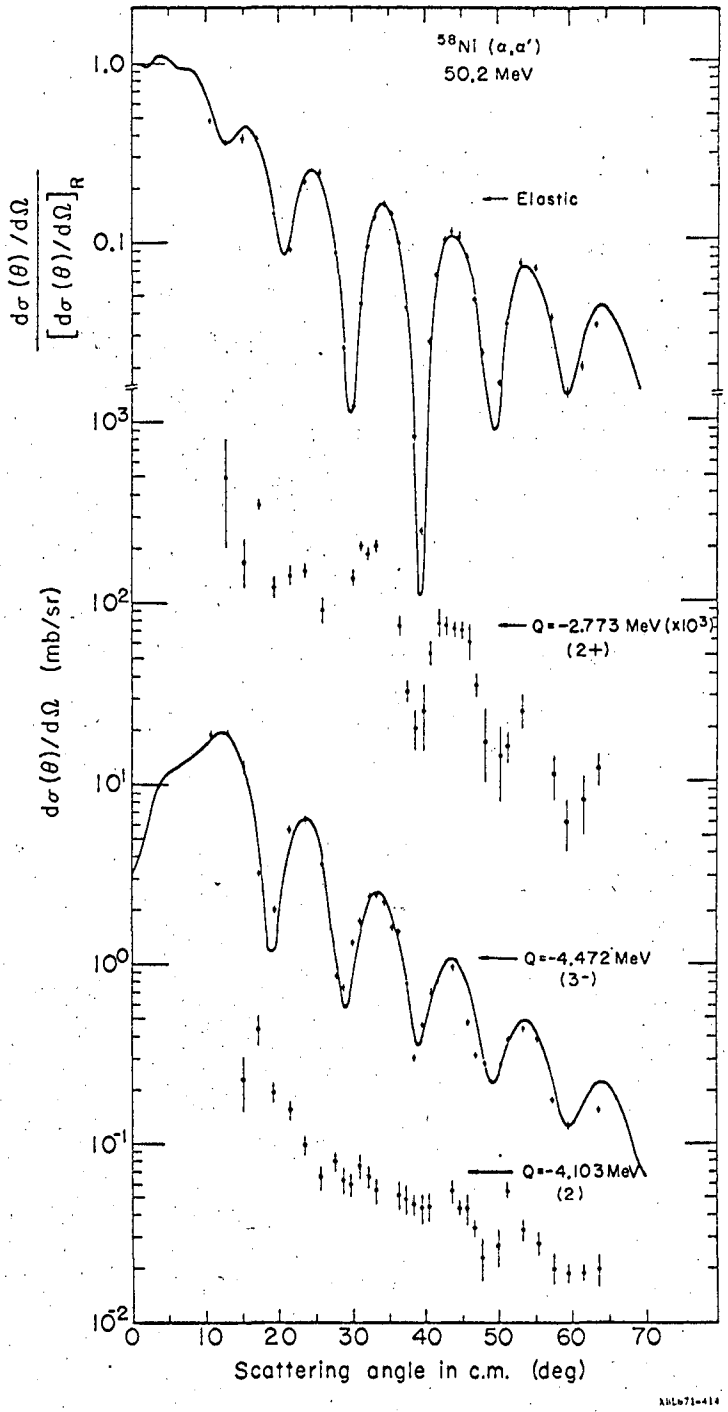
^{58}Ni (α,α')
50.2 MeV
Elastic
Q=-2.773 MeV (x10^3)
(2+)
Q=-4.472 MeV
(3-)
Q=-4.103 MeV
(2)
$\frac{d\sigma(\theta)/d\Omega}{[d\sigma(\theta)/d\Omega]_R}$
$d\sigma(\theta)/d\Omega$ (mb/sr)
Scattering angle in c.m. (deg)

Fig. 11(a).

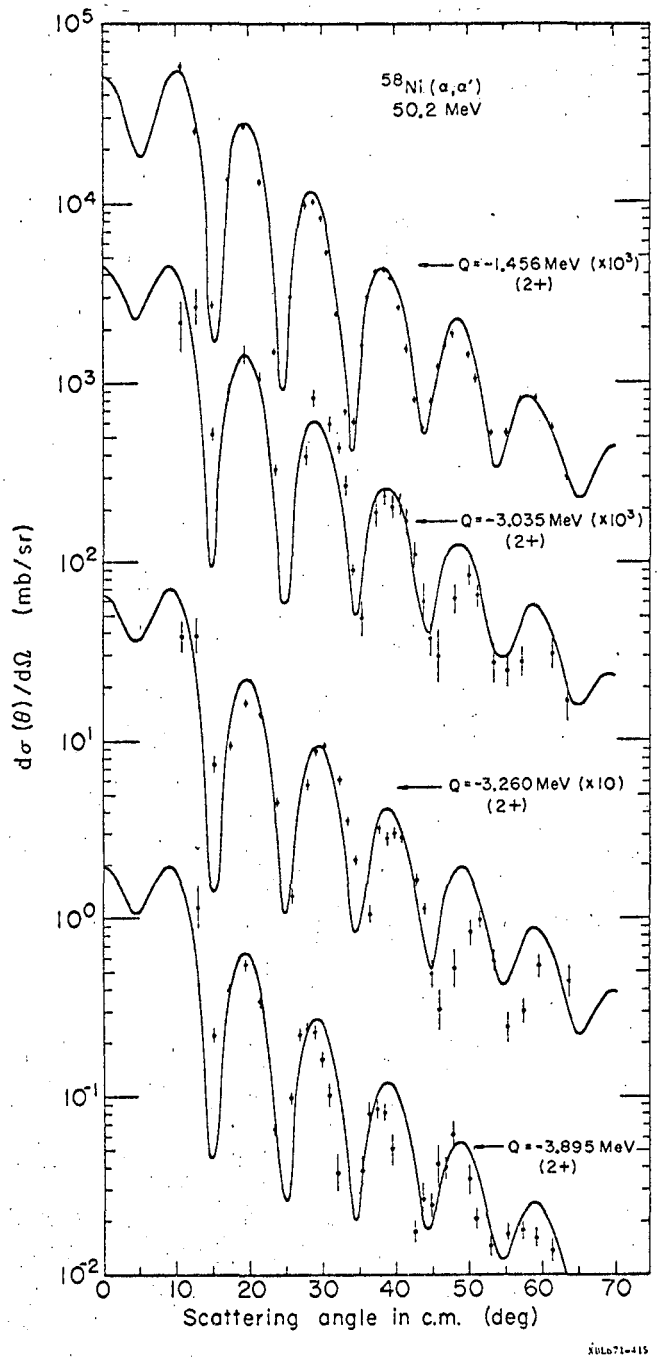
^{58}Ni (α,α')
50.2 MeV
Q=-1.456 MeV (x10^3)
(2+)
Q=-3.035 MeV (x10^3)
(2+)
Q=-3.260 MeV (x10)
(2+)
Q=-3.895 MeV
(2+)
dσ (θ)/dΩ (mb/sr)
Scattering angle in c.m. (deg)
XBLo71-415

Fig. 11(b).

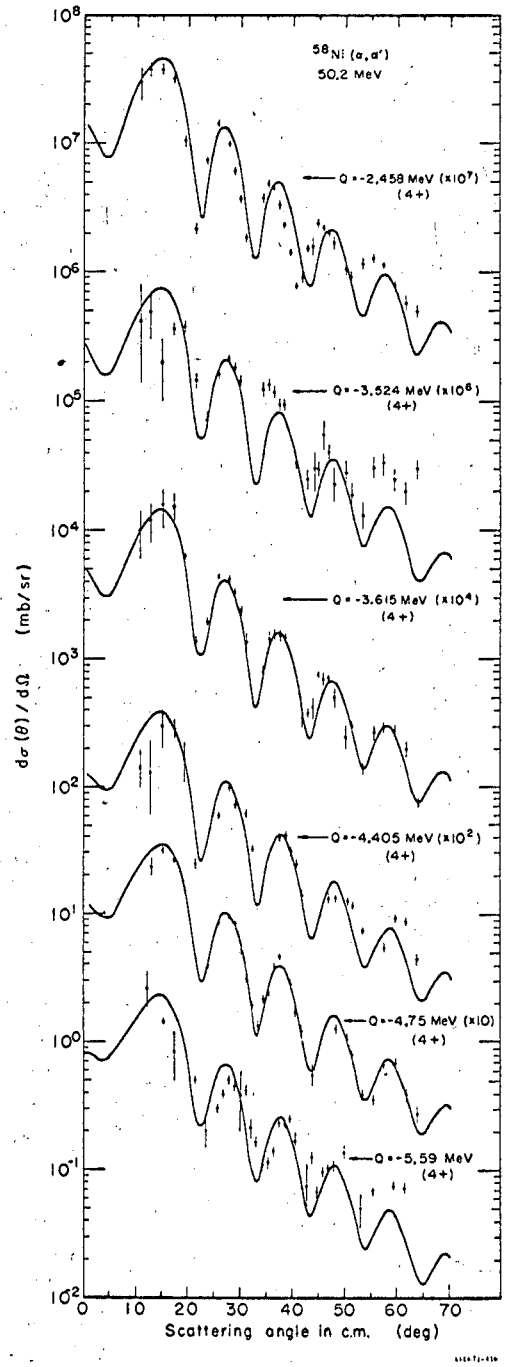
58Ni (α, α')
50.2 MeV
Q = -2.458 MeV (x10^7)
(4+)
Q = -3.524 MeV (x10^6)
(4+)
Q = -3.615 MeV (x10^4)
(4+)
Q = -4.405 MeV (x10^2)
(4+)
Q = -4.75 MeV (x10)
(4+)
Q = -5.59 MeV
(4+)
dσ(θ) / dΩ (mb/sr)
Scattering angle in c.m. (deg)

Fig. 11(c).